Burst Detection and Location in Pipelines and Pipe Networks

with application in water distribution systems

Dalius Misiunas

LUND UNIVERSITY

Licentiate Thesis
Department of Industrial Electrical Engineering
and Automation

Department of
Industrial Electrical Engineering and Automation
Lund University
Box 118
SE-221 00 LUND
SWEDEN

http://www.iea.lth.se

ISBN 91-88934-30-6
CODEN:LUTEDX/(TEIE-1038)/1-290/(2003)

Printed in Sweden by Universitetstryckeriet
Lund University
Lund, 2004

Abstract

Sudden pipe bursts occur in high-pressure water transmission pipelines and water distribution networks. The consequences of these bursts can be very expensive due to the outage time while the burst pipe is repaired, the cost of repair, and damage to surrounding property and infrastructure. As a result, it is advantageous to minimise the detection and location time after the burst occurs.

Currently, there is no effective solution for the burst detection and location problem in water distribution systems. The applications in oil and gas pipelines and pipe networks show the advantages of continuous monitoring. A number of techniques are used to determine the location and size of a burst. One of the most promising approaches is fluid transient modelling and analysis. Pressure transient analysis has also been successfully applied for detection and location of existing leaks.

A sudden pipe burst creates a negative pressure wave that travels in both directions away from the burst point. The analysis of this wave is the main principle for the techniques presented in this thesis. Experiences from previous research suggest that, to achieve the best performance, single pipelines and pipe networks have to be treated separately. Thus, two different approaches for burst detection and location are presented.

When a burst occurs in a pipeline, the burst-induced pressure wave travels in both directions along the pipeline and is reflected at the boundaries. Using a pressure trace measured at one location along the pipeline, the timing of the initial and reflected burst-induced waves determines the location of the burst. The presented continuous monitoring technique uses the modified two-sided cumulative sum (CUSUM) algorithm to detect abrupt changes in the pressure

data caused by the pipe break. The results from both laboratory and field pipelines are used to verify the proposed method. Different burst and measurement locations are tested. The results are promising for burst detection and location in real systems.

In the network case, continuous pressure measurements at two locations are analysed. The burst detection and location algorithm is based on the difference between the arrival times of the burst-induced pressure wave at each measurement point and on the measured wave magnitude. The arrival times are determined automatically in real time. A method for determining optimal measurement locations is also presented. Results from numerical simulations show that the proposed technique has potential as a tool for effective detection and location of bursts in real pipe networks.

Most transient-based techniques use transient modelling for analysis or validation. The development of a transient model comprises part of the work presented in this thesis. The Method of Characteristics is used to solve the governing unsteady flow equations. Models for unsteady friction, leakage and burst are included. The model is used to validate the results of burst detection and location.

Acknowledgements

First of all, I would like to express my most sincere gratitude to my supervisor Professor Gustaf Olsson, who has given me the opportunity to undertake this work. His optimism and ability to put things into perspective has been a great source of inspiration. I also want to thank Gustaf for his trust and encouragement.

The Department of Industrial Electrical Engineering and Automation is a great place to work. I want to thank all of the people in the department for contributing to a good working environment. I would especially like to express my gratitude to: Inés for being a great friend, Christian for help with LaTeX code, Christian and Ulf for reading the manuscript, Gunnar for solving computer problems, Anita and Christina for doing the paper work, and Carina and Getachew for their help with practical things.

Six months spent at the Centre for Applied Modelling in Water Engineering, School of Civil and Environmental Engineering, the University of Adelaide, Australia were both interesting and fruitful. I would like to thank Associated Professor Angus Simpson and Dr. Martin Lambert for this great opportunity to be a part of the "transient" group.

Dr. John Vítkovský has been a great teacher and colleague, his clear answers and critical view are highly appreciated. I want to thank Mark, Pedro and Young Il for making laboratory and field work fun. I also want to thank all people at the School of Civil and Environmantal Engineering for creating a warm and friendly atmosphere. Especially Greer, for making me feel at home.

I also wish to thank all of my friends who have been with me through this time. Without them it would be hard to survive through the bad weather or approaching deadlines. I am grateful for all the happy moments we have had together.

Finally, I would like to thank my parents and my brother for their love and understanding. Although being far away, they have always been a great support.

This work was partially supported by VINNOVA, Per Westling fund, The Royal Swedish Academy of Sciences and Kung. Fysiografiska Sällskapet i Lund. The support is greatly acknowledged.

Lund, November 30, 2003
Dalius Misiunas

Contents

Chapter 1

Introduction

1.1 Motivation

The present state of the urban water supply infrastructure is a result of hundreds of years of development and large investments. The size, cost and complexity of today's water distribution systems prevent radical changes and straightforward applications of modern techniques. The environmental concerns over the last few decades, together with increased awareness of customers, have placed pressure on water utilities to improve water services. This pressure is supported by the rapid development of advanced technologies in instrumentation, control and computer applications. Although considerable effort has been made to advance the operation of water distribution systems, water supply still remains one of the most stagnant parts in the urban infrastructure system.

Water is a precious resource and is essential for human existence. Therefore a special concern has been expressed by policy makers with the emphasis on the conservation of natural recourses. New legislation has raised higher demands for the efficiency of water supply in many countries. Moreover, there are indications that water policies will become even stricter in the near future. This situation forces water utilities to look for ways to improve the existing water supply systems. Reducing losses and increasing the reliability of the service are amongst the most important tasks.

1.2 Objectives

This research project was initiated with a very broad objective – to improve the operation of urban water supply by utilising available resources and technology. During the initial stage, a number of problems that were of greatest concern from the water industry's point of view were identified (Misiunas; 2001a,b,c,d). As a result, the following objectives were formulated: (1) Explore the possibilities of system monitoring for fault detection and location. The pipe breaks can be referred to as one of the most frequent types of fault; (2) Find techniques that would utilise the existing (or inexpensive to obtain) measurements from the water distribution network in the most efficient way. In other words, to extract the important information about the state of the system from the measured data; (3) Analyse the possible application of these techniques in both a single pipeline and a pipe network situation.

1.3 Contributions

The contributions of this thesis are presented in Chapter 7. A brief summary of the main results is given here:

- A new approach for sudden burst detection and location in fluid pipelines is presented. It is based on the continuous monitoring of pressure at a single point along the pipeline and transient analysis of the measured signal.
- A new technique for burst detection and location in pipe networks is derived. The pressure is monitored at two or more points throughout the network and the location of the burst is determined from the timing of the burst-induced transient wave.
- An algorithm for analysis of measured pressure data is derived. It is used to detect changes in pressure time series that are caused by the burst-induced transient wave.
- A hydraulic transient simulation tool is implemented. Governing equations of unsteady flow are solved using the Method of characteristics. Unsteady friction model is included into the solver.

1.4 Outline of the thesis

In Chapter 1, the motivation, objectives and main contributions of this thesis are presented.

In Chapter 2, the problem of pipe bursts in water distribution systems is discussed. The reasons for having an effective burst detection and location mechanism and requirements for such a system are presented.

In Chapter 3, a review of existing methods for burst detection and location is presented. Techniques used in water distribution systems and in oil and gas industries are described. The approaches for transient leakage detection are also explained.

In Chapter 4, a simulation model for transients in pipe networks is described. The transient model is based on the Method of Characteristics. A number of different implementation aspects are discussed throughout the chapter.

In Chapter 5, a new technique for detecting and locating sudden bursts in pipelines is presented. The methods for burst location and estimation of size are explained. Results from experimental validation in both the laboratory and field are presented. Limitations of the approach are discussed.

In Chapter 6, a new approach for sudden burst detection and location in pipe networks is presented. An algorithm for deriving the burst location and size is explained. A method for selecting measurement positions is described. Validation on a small scale network is performed using simulated burst data. Limitations are discussed.

In Chapter 7, general conclusions are made and directions for the future work are presented.

Three appendices are included at the end of the thesis. The experimental work is described in Appendix A. In Appendix B, the equations for calculating transient wave transmission coefficients for junction and basic boundaries are derived. Finally, Appendix C illustrates the derivation of the burst size equation.

1.5 Publications

International conference publications

Misiunas, D., Vítkovský, J., Olsson, G., Simpson, A. and Lambert, M. (2003). Pipeline burst detection and location using a continuous monitoring technique, *International Conference on Advances in Water Supply Management, CCWI*, 15-17 September, 2003, Imperial College, London, UK.

Misiunas, D., Vítkovský, J., Olsson, G., Simpson, A. and Lambert, M. (2004). Burst detection and location in pipe networks using a continuous monitoring technique, *9th International Conference Pressure Surges*, 24-26 March, Chester, UK, (accepted for publication).

Technical reports

Misiunas, D. (2001). Drinking water quality. Literature study on water distribution systems, *Technical report TEIE-7169*, Dept. of Industrial Electrical Engineering and Automation, Lund University, Lund, Sweden.

Misiunas, D. (2001). Dynamic behavior of a pump/pipeline system. Literature study on water distribution systems, *Technical report TEIE-7166*, Dept. of Industrial Electrical Engineering and Automation, Lund Univer-sity, Lund, Sweden.

Misiunas, D. (2001). Leakage control. Literature study on water distribution systems, *Technical report TEIE-7167*, Dept. of Industrial Electrical Engineering and Automation, Lund University, Lund, Sweden.

Misiunas, D. (2001). Water storage. Literature study on water distribution systems, *Technical report TEIE-7168*, Dept. of Industrial Electrical Engineering and Automation, Lund University, Lund, Sweden.

Misiunas, D. (2002). Integrated information and operation systems in urban water infrastructure - leakage control, *Technical report TEIE-7172*, Dept. of Industrial Electrical Engineering and Automation, Lund University, Lund, Sweden.

Chapter 2

Bursts in water distribution systems

In this chapter, the problem of pipe bursts in water distribution systems is discussed. The water distribution network is a complex and, in many cases, old system. Structural deterioration of pipe networks leads to an increased frequency of pipe breaks. Bursts can be both harmful and expensive to repair. However, the damage due to bursts can be minimised by effective burst detection and location. The main requirements for such technique are presented at the end of the chapter.

2.1 The structure of water distribution systems

Although the size and complexity of the drinking water distribution systems vary dramatically, they all have the same basic purpose – to deliver water from the source (or treatment facility) to the customer. The objectives of an urban water system are to provide safe, potable water for domestic use, adequate quantity of water at sufficient pressure for fire protection, and water for industrial use. A typical waterworks consists of source-treatment-pumping and distribution system. Sources for municipal supplies are wells, rivers, lakes and reservoirs. About two thirds of the water for public supplies comes from surface-water sources. Often groundwater is of adequate quality to preclude treatment

other than chlorination and fluoridation. The drinking water distribution system basically consists of a series of pipes joined to each other by nodes. When links and nodes constitute closed paths, they form loops. The water to the network may be supplied by sources, by fixed head nodes, such as reservoirs, or by a combination of both. Moreover, the network may contain pumps and hydraulic fittings, such as bends and valves.

Transmission and distribution mains

The system of piping is often categorized into transmission/trunk mains and distribution mains. Transmission mains consist of components that are designed to convey large amounts of water over great distances, typically between major facilities within the system. For example, a transmission main may be used to transport water from a treatment facility to storage tanks throughout several cities and towns. Individual customers are usually not served from transmission mains.

Distribution mains are an intermediate step towards delivering water to the end customers. Distribution mains are smaller in diameter than transmission mains and typically follow the general topology and alignment of the city streets. Elbows, tees, crosses, and numerous other fittings are used to connect and redirect sections of pipe. Fire hydrants, isolation valves, control valves, blow-offs and other maintenance and operational appurtenances are frequently connected directly to the distribution mains. Services, also called service lines, transmit the water from the distribution mains to the customers.

Households, businesses and industries have their own internal plumbing systems to transport water to sinks, washing machines, and so forth.

System configuration

Transmission and distribution systems can be either looped or branched. As the name suggests, in a looped system there might be several different paths that the water can follow to get from the source to a particular customer. In a branched system, also called a tree or dendritic system, the water has only one possible path from the source to a customer.

Looped systems are generally more desirable than branched systems because, coupled with sufficient valving, they can provide an additional level of reliability. Another advantage of the looped configuration is that, because there is more than one path for water to reach the user, the velocities will be lower, and system capacity greater. Most water supply systems are a complex combination of loops and branches, with trade-offs between loops for reliability (redundancy) and branches for infrastructure cost savings.

2.2 System deterioration

The water networks serving the utilities in Western Europe and North America are up to 150 years old. The older parts of the networks were built below the current standards and construction practises, and with technologies that are no longer appropriate. Nevertheless, to replace these parts of the networks is generally beyond the economic capabilities of the water utilities.

As water mains deteriorate both structurally and functionally, their breakage rates increase, network hydraulic capacity decreases, and the water quality in the distribution system may decline. The deterioration of the pipes can be classified into two categories (Kleiner and Rajani; 2001). The first is structural deterioration, which diminishes the pipes structural resiliency and their ability to withstand the various types of stresses imposed. The second is the deterioration of inner surfaces of the pipes resulting in diminished hydraulic capacity, degradation of water quality and reduced structural resiliency in the case of severe internal corrosion.

2.3 Losses in water distribution systems

Different definitions of losses in water distribution systems can be found in the literature. The terminology used here is suggested by the International Water Association (EUREAU; 2001; Lambert and Hirner; 2000).

The most basic way to determine losses in to calculate the difference between the system input and output. These losses can be divided into “apparent losses” and “real losses”. Apparent losses are caused by unauthorised consumption by

illegal connections and metering inaccuracies. Real losses are caused by leakage and overflows. The term Unaccounted For Water (UFW) describes the combination of real and apparent losses.

Leakage

Leakage from the water distribution pipeline network can be defined as that water which, having been obtained from the source, treated and put into supply, leaks and escapes other than by a deliberate action. In the UK, between 20% and 30% of transported water was lost through leakage during the 1990s (OFWAT; 2001). This figure can be even higher for older pipes. The loss of such large volumes of water is environmentally and economically damaging. The AWWA manual "Water Audits and Leak Detection" (AWWA; 1999) lists six main sources of leakage that may occur in any section of the system:

- Material defects induced by poor design or insufficient planning at the concept stage.
- Pipe breaks caused by poor workmanship in the construction phase – laying and support of pipes.
- Operational errors – overpressure, water hammer, valve operation, etc.
- Corrosion due to soil and/or water chemistry effects and groundwater effects (e.g., seawater).
- Leakage from any of the installed fittings (valves, saddles, bends, tees, hydrants, etc.).
- Accidental or deliberate damage of hydrants and line air valves (including unauthorized tappings).

Two types of leakage can be defined depending on the magnitude of the leak flow and on the way the leak flow develops. The first type can be referred to as slow leaks. A leak of this type is usually of small size at the moment when it occurs and develops gradually over time. The second type of leaks are sudden bursts with a greater leak flow. The burst is usually a result of a pipe or joint break.

Pipe material	Length, %	# of breaks/100 km/year
Cast iron	50	35.9
Ductile iron	24	9.5
Asbestos-cement	12	5.8
PVC	10	0.7

Table 2.1: Water main break data.

Pipe breakage rate

One common indicator of water distribution systems deterioration is the number of water main breaks. Two-year pipe break data from 21 Canadian cities are presented in Rajani and McDonald (1995). This data were analysed with regard to the type of pipe material and the proportional representation of the particular material in the total water distribution system. A summary of the collected data is presented in Table 2.1

Pelletier et al. (2003) conducted a study based on annual pipe break statistics and the perception of water managers. A ratio of 40 or more breaks per 100 km per year is considered to be high and indicates a network in poor condition. Networks with ratios between 20 and 39 annual breaks per 100 km are considered to be in acceptable condition, while ratios less than 20 annual breaks per 100 km indicate that the network is in good condition.

Several authors (Khomsi et al.; 1996; Loganathan et al.; 2002) have derived models for predicting pipe burst rate. The results of these studies show that break ratio is proportional to the age of the pipes. This means that the frequency of bursts is expected to increase in the future.

2.4 Motivation for burst detection and location

The rapid development of different components of urban infrastructure system over last few decades has created a strong pressure for water utilities. The demand for a high quality water services has increased. Yet, at the same time, water supply systems are deteriorating due to the ageing of pipes. As water

distribution systems are getting older, burst rates increase. The economic and social costs associated with pipe bursts are rapidly rising to unacceptably high levels. These costs can be classified as follows:

- *Lost water*. The volume of water lost until the damaged pipe section is isolated after the burst has occurred can be considerably large. The cost of lost water varies depending on the water resources available. However, it has to be noted that it is treated water being lost and therefore the treatment cost needs to be considered.

- *Interrupted supply*. The burst event introduces certain changes to the hydraulic state of the system. Losses through the burst can decrease the pressure in the pipeline or network section to an insufficient level. The service might be interrupted at a number of connection points. In case of transportation main burst, a considerable number of consumers can be left without water.

- *Structural damages*. Pipe bursts can be extremely harmful for the surrounding infrastructure. Large bursts can cause flooding of streets and houses, and the collapse of roads and pavements due to foundation washou

- *Repair costs*. Depending on the size and duration of the burst, repair costs can become high. The restoration of damaged burst surroundings, compensation for lost property are the costs that have to be added on top of the amount spent for pipe repair.

The consequences of pipe bursts listed above can be both expensive and harmful and therefore are highly undesirable. The overall damage caused by a burst depends on the time between the actual event and its isolation. To minimise the costs associated with pipe failure a technique for quick burst detection and location is necessary. In the following section the main requirements for such technique are addressed.

2.5 Requirements for burst detection and location technique

Detection and location of bursts in a water distribution systems is a complicated task. A compromise between cost and performance has to be reached. The following requirements can be formulated for an effective burst monitoring system:

- *Continuous operation*. The time of pipe failure is highly unpredictable. Therefore, the monitoring system should be active at all times.
- *Short response time*. It is essential to minimise the time from the burst event until the broken pipe (or its section) is isolated.
- *Low installation and maintenance costs*. The investments that can be made by water companies are limited. Therefore the system requiring the least amount of instrumentation is preferred.
- *Low false alarm rate*. Legitimate increase in demand or pressure oscillation caused by pump operations should be recognised and ignored.
- *Burst and leak detection*. Both bursts which occur instantly and leaks which develop gradually should be detected.
- *Online data analysis*. For a quick reaction online data analysis is necessary. The burst position and size should be determined automatically.

Chapter 3

Burst detection and location techniques

In this chapter, techniques for burst detection and location are discussed. The review of techniques can be divided into three parts: (1) the current practise in water industry, (2) techniques used in oil and gas industries, and (3) transient-based methods used for detecting existing leaks. A summary of all methods and conclusions is given at the end of the chapter.

3.1 Static mass balance

In present practise of water companies, the most common technique for identifying leakage is to conduct a water audit. A detailed account of water flows into and out of the distribution system, or parts of it, is recorded. At the level of the whole system, this consists of a total water supply balance, i.e. the summation of water consumed (metered and unmetered) and not consumed (leakage, theft, exports etc.) compared with the total distribution input. District flow metering extends this to monitoring individual zones. The distribution system is subdivided into discrete zones, or district meter areas (DMA), by the permanent closure of valves. A DMA will generally comprise 500-3000 properties. Flow (and sometimes pressure) sensors are placed on the DMA boundaries and collected data are subsequently analysed for leakage trends. The most popular

operational use of the flow data is the analysis of measured minimum night flows. Night flows (usually measured between midnight and 5:00 am) are used because the water usage is at its minimum and it is easier to identify and subtract legitimate flows. Any remaining unusual changes in volumes will signify leakage in the absence of any other factors. If it is established that the leakage has increased sufficiently to warrant further investigation, then a manual leakage detection is carried out on the entire DMA using methods such as step testing, sounding and leak noise correlation (Golby and Woodward; 1999). This detection takes approximately one day per 350 properties for one leakage team.

Supervisory control and data acquisition systems (SCADA) are used for monitoring flows at critical points in the system. In general, flow sensors log the flow every 15 minutes. The possibility to collect data online slightly improves the performance of leakage detection. However, present systems do not include an algorithms for evaluating sensor data and deriving leakage levels.

In Mounce et al. (2003) and Mounce et al. (2001) an extension of the DMA approach is described. The approach is based on analysis of data fusion for sensors measuring hydraulic parameters (flow and pressure) within the DMA. A neural network knowledge-based system was developed for automatic and continuous monitoring of the measured data for normal and abnormal behavior. As a part of the same work, Khan et al. (2002) developed a low-cost failure sensor design. The design of sensors was based on correlation between abnormal flows and the opacity of the water. Sensors were placed within the DMA and measured the opacity of the water flow. The leak was identified from the sensor data.

3.2 State estimation

A number of state estimation approaches for burst detection and location are described in the literature (Andersen and Powell; 2000; Poulakis et al.; 2003; Tao and Wang; 1988). The general idea of such a methodology is to estimate the current values of state variables (pressure, flow, nodal demands), given fixed network parameters. The procedure is often carried out at snapshot instances in time. To give a better understanding of the methodology, two different approaches of state estimation are described below.

In Andersen and Powell (2000), the implicit formulation of the standard weighte least squares (WLS) state-estimation problem for water networks with a low measurement redundancy is presented. The formulation is based on loop equations (instead of nodal) and the state variables are unknown nodal demands. The ultimate possibility of leak node identification in the case of no network uncertainties and measurement errors was demonstrated for an idealised network example. However, it was noted that in practical applications, network uncertainties and measurement errors would be abound for obtaining the correct solution.

Another system identification approach was employed for leakage detection by Poulakis et al. (2003). The Bayesian methodology used in this study handles the uncertainties in measurement and modelling error. Again, a simulated data were used for testing. Two types of measuring devices were considered - manometers and flow meters. The model errors were introduced by perturbation of pipe roughness, flow demands at nodes and measurements. The results showed that the algorithm is quite sensitive to the errors in parameters and measurements. Perturbations of more than 5% were shown to cause poor performance of the method.

3.3 Statistical analysis

The statistical method for detecting and locating pipe breaks does not use mathematical models to calculate flow or pressure in a pipeline, but rather detects changes in the relationship between flow and pressure using available measurement data. An example of a statistical pipeline leak detection system is described in Zhang (2001). An optimum sequential analysis technique (Sequential Probability Ratio Test) was applied to detect changes in the overall behavior of inlet and outlet flow and pressure. The measurements were performed with a 30 s sampling interval. The system was implemented on a 37 km long propylene pipeline and was shown to detect 1% leaks with less than 20% error in position. The detection time was less than 20 minutes.

In Wang et al. (1993), a method of leak detection based on autoregressive modelling was proposed. This method requires four pressure measurements, two at each end of the pipeline. A leak is detected by analysing the time sequences

of the pressure gradient at the inlet and outlet of the pipeline. A sampling frequency of 50 Hz was used in the study. It was shown that a 0.5% leakage in a 120 m long pipe can be reliably and almost instantly detected by this method.

3.4 Transient modelling

Using real-time data from a SCADA system as boundary conditions, a real-time transient flow simulator can be an effective tool for monitoring abnormalities in pipelines. Several methods based on a fluid transient model are found in the literature. Most of them are applied in oil and gas industry. Two different approaches are described – a pressure discrepancy method and a dynamic volume balance method (Kiuchi et al.; 1995). Both approaches use the analysis of discrepancies between simulated and measured data. The pressure discrepancy method compares pressure values at a number of points throughout the system. In the dynamic volume balance method, two flow discrepancies are computed at the inlet and outlet (Kiuchi; 1993; Liou and Tian; 1995). This method uses the fault sensitive approach – the pipeline is assumed to be intact in the calculations. The real-time pressure and flow measurements at both ends of the pipeline are collected with a sampling interval of 15-30 s. The measured pressure and flow are used as boundary conditions in a transient model. When the leak occurs, it is manifested in the measurements. Thus, the simulated flow and pressure values diverge from the measured ones. The average response time of the method is expected to be less than one hour.

Benkherouf and Allidina (1988) describe a fault model approach for leak detection in gas flow pipelines. The method is based on a discrete Kalman filter for the nonlinear distributed parameter system representing the gas flow in a leaking pipeline. The Method of Characteristics was applied to lump the distributed parameter system. Is was assumed that measurements of pressure at discrete points along the pipeline were available. Artificial leak states at predefined positions along the pipeline were included in the filter model and relationships for estimating the actual leak position were derived. Results from the simulated case show that the actual position of a 2% leak could be obtained approximately 80 min after the occurrence of the leak when two or three pressure measurements were used in a 90 km long gas pipeline. Time step values of 7.5 s and 100 s were used for generating measurement data.

3.5 Transient analysis

The occurrence of a sudden leak in a pipeline causes a pressure decrease which is followed by a transient wave travelling upstream and downstream along the pipeline. The analysis of this burst-induced wave can be used for leak detection and location. In Silva et al. (1996), an approach using four continuous pressure measurements along the pipeline was presented. The sampling frequency of 2000 Hz was used. Pressure data were used to first calculate the wave speed and then derive the leak position. Results from two experimental (433 m and 1248 m long) pipelines showed that the precision of leak location estimates depends on the leak size and the distance from the leak to the nearest transducer. Different leak sizes (5-50%) were tested and errors in burst location below 10% were observed.

3.6 Fluid transient leak detection

A number of techniques for detecting and locating existing leaks are described in the literature. These approaches are used for system diagnostics rather than continuous monitoring. In other words, the periodical checks are made to evaluate the state of the system and identify existing faults. The main objective of all transient leak detection methods is the same – extract the information about the presence of the leak from the measured transient trace. For the generation of a transient event, system elements (i.e. inline valves and pumps) or special devices (such as solenoid side discharge valves) are used. The fact that the transient wave speed can be over 1000 m/s means that a high sampling frequency of pressure measurements is required. The choice of measurement position and the characteristics of generated transients depend on the method that is used for further analysis.

The leak reflection method (Brunone; 1999; Brunone and Ferrante; 2001; Jönsson and Larson; 1992; Jönsson; 1995, 2001) is probably the most straightforward and simple application of transient analysis for leakage detection. A transient wave travelling along the pipeline is partially reflected at the leak. If the reflected wave (usually the first reflection is considered) can be identified in a measured pressure trace, the location of the burst can be found using simple

calculations. This method is based on the principle of time domain reflectometry (TDR). TDR is a well-established technique in electric power systems (Cowan; 1975; Harding; 1976). For the best results, a sharp transient wave has to be used. The detection of change in the measured pressure caused by leak reflection can be difficult. In Lee et al. (2003a), the cumulative sum algorithm is used to evaluate the discrepancy between measured and simulated (intact pipe) data. The application of the leak reflection method is limited to the single pipe case.

The inverse transient method (ITM) (Liggett and Chen; 1994) uses least squares regression between modelled and measured transient pressure traces. The leak is modelled at discrete positions (usually nodes) in the network and the minimisation of the deviation between the measured and calculated pressures produces a solution of leak location and size. In addition to leak detection, ITM can be used for any system parameter calibration, given enough measurement data. Nash and Karney (1999) presented an application of ITM for a series-connected pipelines. To improve the efficiency of optimisation, a genetic algorithm search method was implemented into ITM (Vítkovský et al.; 1999, 2001). Experiences from real tests indicate that the challenge for applying ITM is the accurate modelling of the transients and boundary conditions in a pipe network.

The transient damping method (Wang et al.; 2002) uses the damping rate of the transient trace to detect a leak. The decay of the transient wave is caused by pipe friction and leaks. Leaks can be detected by comparing the measured pressure containing the leak-induced damping to the simulated results for the same pipeline without a leak. The possibility of applying this method in pipe networks has not been investigated.

The frequency response method (Ferrante and Brunone; 2003a,b; Lee et al.; 2003b) uses the analysis of transient response in the frequency domain. Fourier transforms are used to transform time-domain data into the frequency domain. By comparing the dominant frequencies of no-leak and leaking pipelines, the leak location can be obtained. Performance of the method is strongly influenced by the shape of the transient and the measurement location. Only pipeline applications of frequency response analysis are presented in literature.

3.7 Acoustic methods

As an alternative to the model-based techniques described above, acoustic measurements can be used to detect and locate leaks. An acoustic signal generated by the escaping leak mass propagates through the flowing fluid or through the pipeline wall. The complexity of acoustic systems varies from manual checks using geophones to permanent continuous monitoring systems (Rajtar and Muthiah; 1997). Acoustic leak detection systems have been successfully applied to detect and locate defects in nuclear power plants, petroleum and chemical systems and water distribution systems. However, according to the review of leak detection methods presented in Wang et al. (2001), there are several disadvantages of acoustic methods. Factors that affect the performance of acoustic leak detection and location are: (1) unwanted interference noise (traffic, wind, etc.), (2) varying sound propagation conditions from one pipeline section to another, (3) characteristics of the leak (i.e. large pipe burst surrounded by the water that has escaped the pipe produces weak signal), (4) multiple leaks tend to give incorrect leak locations and (5) strong acoustic damping in plastic pipes.

3.8 Summary and conclusions

Some general conclusions can be made from the review presented in this chapter.

- Quick burst detection and location cannot be achieved with techniques currently used in water industry. As a result, bursts are often detected visually after the water appears on the ground surface.

- Most of the existing burst (leak) detection and location techniques can be used only for single pipelines. Only a few methods were applied in pipe networks. This suggests that the pipeline and network situations have different characteristics and different methods have to be applied.

- Techniques using dynamic modelling and real-time data generally have better performance than the static analysis applications. This is primarily indicated by shorter response time. The precision of the estimated position and size of the burst is also higher when using dynamic analysis.

- The data availability and sampling frequency of measurements are important factors influencing the performance of the monitoring technique. Having more measurement points improves the precision and reliability of the results.

- Fluid transient analysis has proven to be the unique source of information about the physical state of the pipe. The fact that only pressure measurements can be used for the analysis is an advantage. Pressure transducers are less expensive and easier to maintain than flow meters.

- An accurate transient model can improve the performance of leak and burst detection techniques. The modelling can be used as a part of the analysis procedure or as a tool to verify obtained results.

Chapter 4

Fluid transient modelling

In this chapter, the details of a computer simulation model based on the Method of Characteristics for modelling transients in pipelines and pipe networks are presented.

4.1 Introduction

Transient analysis can be identified as one of the most promising techniques for detecting and locating failures in pipelines and pipe networks. Most of the transient-based techniques use transient modelling as one of the main parts in the analysis. Thus, having an accurate transient model is important.

Recently, a number of commercial software packages for transient simulation in water distribution pipelines and networks were introduced to the market. The use of these tools for research purposes is limited. The main restriction is the fact that no changes can be made in the source code, which means that modification of existing and implementation of new elements (such as boundary conditions or unsteady friction models) is prohibited. Therefore, as a part of the work described in this thesis, a hydraulic transient model was implemented.

4.2 Model implementation

The Method of Characteristics (MOC) is used for solving governing unsteady flow equations. The computer code is written in C++ programming language. The transient model is integrated with EPANET steady state hydraulic solver (Rossman; 2000), which is employed for simulating steady state flow in the network to establish the initial flow conditions for the transient simulation. Another important feature is the graphic user interface offered by EPANET. A network model is created and modified in a quick and convenient way. The model input files from most of the commercial software packages are compatible with EPANET.

4.3 Governing equations

Unsteady state flow in a closed conduit can be described by equations derived from the principles of conservation of mass and linear-momentum. The detailed derivation of governing equations is not demonstrated in this section, but can be found in Wylie (1983). The following simplified form of the continuity and motion equations is most commonly used

$$\frac{\partial H}{\partial t} + V\frac{\partial H}{\partial x} + \frac{a}{gA}\frac{\partial Q}{\partial t} = 0 \tag{4.1}$$

$$\frac{1}{gA}\frac{\partial Q}{\partial t} + \frac{V}{gA}\frac{\partial Q}{\partial x} + \frac{\partial H}{\partial x} + \frac{fQ|Q|}{2gDA^2} = 0 \tag{4.2}$$

where:

H	=	hydraulic head
Q	=	volumetric flow rate
V	=	mean velocity of the flow
g	=	gravitational acceleration
x	=	distance along the pipe
t	=	time
a	=	wave speed in a conduit
f	=	friction factor
D	=	pipe diameter
A	=	cross-sectional area

A number of assumptions were made while deriving the governing unsteady Equations 4.1 and 4.2:

- Liquid flow is one-dimensional and homogenous. Total hydraulic head does not change in the axial direction. Density is constant in the axial direction. Velocity is assumed to be uniform and the average value is used.
- The pipe is horizontal and full at all times.
- Both pipe and fluid are assumed to deform according to linear elasticity.
- Friction is evaluated using the Darcy-Weisbach equation. Unsteady friction loss is assumed to be equal to steady flow friction loss.

4.4 Wave speed in a conduit

In Equation 4.1, the wave speed or celerity, a, is introduced. The wave speed specifies the speed of the pressure disturbance propagation through the fluid in the pipeline. When performing transient analysis, a generalised formula (Wylie and Streeter; 1993) for the wave speed in a thin walled ($D/e > 25$) elastic conduit is

$$a = \sqrt{\frac{\frac{K}{\rho}}{1 + \frac{K}{E}\frac{D}{e}\phi}} \tag{4.3}$$

where:
- K = bulk modulus of elasticity of the fluid
- e = pipe wall thickness
- E = young's modulus of elasticity of the conduit walls
- ρ = fluid density
- ϕ = parameter depending on the pipe anchoring

For the case when a pipe is anchored against longitudinal movement throughout its length, $\phi = 1 - \mu^2$, where μ is the Poisson's ratio of the pipe material.

4.5 Method of characteristics

The Method of Characteristics is currently one of the most popular techniques for solving governing unsteady state equations. The technique is simple and computationally efficient. It is based on the transformation of partial differential equations into ordinary differential equations that apply along specific lines called characteristics. MOC has an extremely flexible solution scheme, which allows fast implementation of models for networks, boundary conditions and non-pipe elements. The discontinuities, such as a fast valve closure, are also handled by MOC.

The governing unsteady pipe flow equations are rewritten as:

$$L_1 = \frac{\partial H}{\partial t} + V\frac{\partial H}{\partial x} + \frac{a}{gA}\frac{\partial Q}{\partial t} = 0 \tag{4.4}$$

$$L_2 = \frac{1}{gA}\frac{\partial Q}{\partial t} + \frac{V}{gA}\frac{\partial Q}{\partial x} + \frac{\partial H}{\partial x} + \frac{fQ|Q|}{2gDA^2} = 0 \tag{4.5}$$

Using the multiplier λ, a linear combination of Equations 4.4 and 4.5 is derived as:

$$\begin{aligned} \lambda L_1 + L_2 = {} & \frac{1}{gA}\left[\frac{\partial Q}{\partial t} + \left(V + \lambda a^2\right)\frac{\partial Q}{\partial x}\right] + \\ & \lambda\left[\frac{\partial H}{\partial t} + \left(V + \frac{1}{\lambda}\right)\frac{\partial H}{\partial x}\right] + \frac{fQ|Q|}{2gDA^2} = 0 \end{aligned} \tag{4.6}$$

The bracketed terms are reduced to form the directional derivatives of Q

$$\frac{dQ}{dt} = \frac{\partial Q}{\partial t} + \frac{dx}{dt}\frac{\partial Q}{\partial x}$$

and H

$$\frac{dH}{dt} = \frac{\partial H}{\partial t} + \frac{dx}{dt}\frac{\partial H}{\partial x}$$

by introducing

$$\frac{dx}{dt} = V + \lambda a^2 = V + \frac{1}{\lambda} \tag{4.7}$$

Equation 4.6 then becomes the ordinary differential equation

$$\frac{1}{gA}\frac{dQ}{dt} + \lambda\frac{dH}{dt} + \frac{fQ|Q|}{2gDA^2} = 0 \tag{4.8}$$

The equality in Equation 4.7 leads to

$$\lambda = \pm\frac{1}{a} \tag{4.9}$$

which, when substituted back into Equation 4.7, yields

$$\frac{dx}{dt} = V \pm a \tag{4.10}$$

Equation 4.10 represents the propagation velocity of a disturbance in a pipe. In water pipes the wave speed is typically three orders of magnitude larger than the velocity of flow. Thus, the flow velocity can be neglected. Equation 4.10 then becomes

$$\frac{dx}{dt} = \pm a \tag{4.11}$$

Equation 4.11 defines two straight lines, called characteristics, along which the variables are differentiated. The characteristic associated with positive a is referred to as the C^+ characteristic, and the C^- characteristic is associated with negative a. Substituting corresponding values of λ into Equation 4.8 leads to two pairs of equations which are grouped and identified as C^+ and C^- equations

$$C^+ : \quad \begin{cases} \dfrac{a}{gA}\dfrac{dQ}{dt} + \dfrac{dH}{dt} + \dfrac{fQ|Q|a}{2gDA^2} = 0 \\ \\ \dfrac{dx}{dt} = +a \end{cases} \tag{4.12}$$

$$C^- : \quad \begin{cases} \dfrac{a}{gA}\dfrac{dQ}{dt} - \dfrac{dH}{dt} + \dfrac{fQ|Q|a}{2gDA^2} = 0 \\ \\ \dfrac{dx}{dt} = -a \end{cases} \tag{4.13}$$

Equations 4.12 and 4.13 are called compatibility equations and are used to

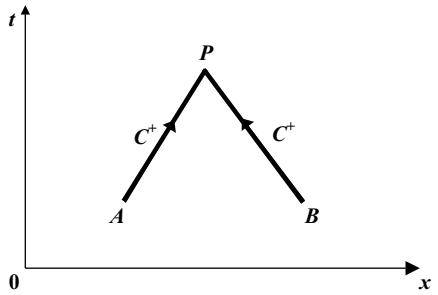

Figure 4.1: Characteristics in the xt plane.

solve for points in the xt plane as shown in Figure 4.1.

The solution of compatibility equations is achieved by integration along the characteristics

$$C^+: \quad \frac{a}{gA}\int_A^P dQ + \int_A^P dH + \frac{fa}{2gDA^2}\int_A^P Q|Q|dt = 0 \qquad (4.14)$$

$$C^+: \quad \frac{a}{gA}\int_B^P dQ - \int_B^P dH + \frac{fa}{2gDA^2}\int_B^P Q|Q|dt = 0 \qquad (4.15)$$

The equations are integrated using an approximation of the friction term (the third term on the left hand side), which restricts results to a small increment in time Δt and space $\Delta x = a\Delta t$:

$$C^+: \frac{a}{gA}(Q_P - Q_A) + (H_P - H_A) + \frac{f\Delta x}{2gDA^2}Q_{AP}|Q_{AP}| = 0 \qquad (4.16)$$

$$C^+: \frac{a}{gA}(Q_P - Q_B) - (H_P - H_B) + \frac{f\Delta x}{2gDA^2}Q_{BP}|Q_{BP}| = 0 \qquad (4.17)$$

where Q_{AP} and Q_{BP} represent the "average" flow along the characteristics during time Δt. Integration of the friction term requires an approximation of the behavior of the flow between end points of characteristics. As suggested by Arfaie et al. (1993), linear approximation is used. The flow at one end of the characteristics is used in one Q-term and the flow at the other end in the other

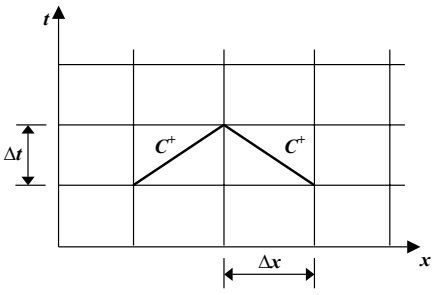

Figure 4.2: xt plane with characteristics grid.

Q-term, which gives:

$$C^+ : \frac{a}{gA}(Q_P - Q_A) + (H_P - H_A) + \frac{f\Delta x}{2gDA^2}Q_P|Q_A| = 0 \qquad (4.18)$$

$$C^+ : \frac{a}{gA}(Q_P - Q_B) - (H_P - H_B) + \frac{f\Delta x}{2gDA^2}Q_P|Q_B| = 0 \qquad (4.19)$$

Research has shown that steady state friction approximations do not generate a sufficient level of damping when compared to experimental results. The introduction of an unsteady friction term causes extra damping and a better fit with experimental data. The implementation of unsteady friction is presented in Section 4.10.

The simultaneous solution of two compatibility equations yields the conditions at a particular time and position in the xt plane designated by point P, given that the conditions at a previous time step are known (points A and B). The grid can be formed of small units (Figure 4.2). This grid is called the characteristics grid.

Two forms of characteristics grid can be used for solving unsteady flow equations - diamond grid or rectangular grid (Figure 4.3). Diamond grid is implemented in the described solver. This choice was based on the fact that, when simulating fast events using rectangular grid scheme, a phenomenon called grid separation introduces an error. Using diamond grid means that the solution at a particular point along the pipeline is obtained every second iteration.

The explicit MOC solution technique is used to solve the characteristics equa-

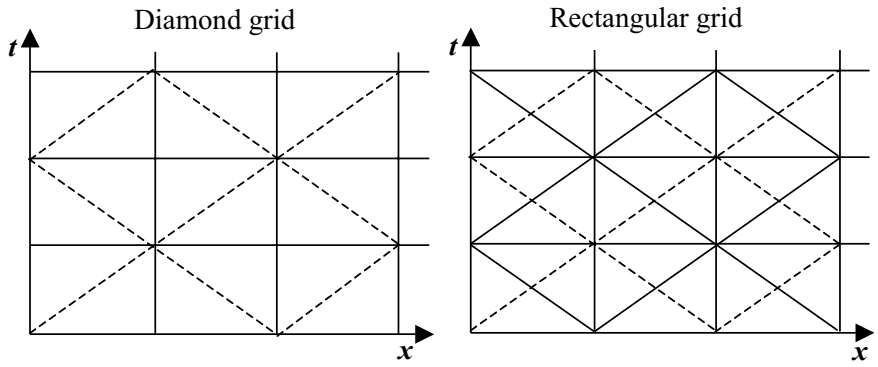

Figure 4.3: Diamond and rectangular grid systems.

tions. This implies that compatibility equations can be solved explicitly and one at a time. By solving for H_P, Equations 4.18 and 4.19 can be simplified, as:

$$C^+ : \ H_P = C_P - BQ_P \tag{4.20}$$

$$C^+ : \ H_P = C_M + BQ_P \tag{4.21}$$

where C_P and C_M are constants that depend on the known conditions at the previous time step

$$C^+ : \ C_P = H_A + Q_A(B - R|Q_A|) \tag{4.22}$$

$$C^+ : \ C_M = H_B - Q_B(B - R|Q_B|) \tag{4.23}$$

B is a function of the physical properties of the pipeline, often called the pipeline characteristic impedance

$$B = \frac{a}{gA} \tag{4.24}$$

and R is the pipeline resistance coefficient

$$R = \frac{f\Delta x}{2gDA^2} \tag{4.25}$$

By first eliminating Q_P in Equations 4.20 and 4.21, H_P is found

$$H_P = \frac{C_P + C_M}{2} \tag{4.26}$$

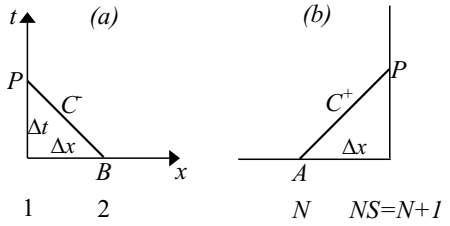

Figure 4.4: Characteristics at boundaries.

Q_P can then be calculated directly from either Equation 4.20 or 4.21. At either end of the single pipe only one of the compatibility equations is available (Figure 4.4). An auxiliary is needed in each case that specifies Q_P, H_P, or some relation between them. That is, the auxiliary equation must convey information on the behavior of the boundary of the pipeline. The boundary conditions for a number of the most common boundaries are defined in literature. In Sections 4.6 and 4.7, the boundary equations for leakage and burst are given special attention, since these boundaries are of the highest significance for the presented research.

4.6 Nodal leakage boundary

A most convenient way of simulating the leakage is assigning it to the nodal points of the characteristic grid. The leaking node is then solved using two compatibility equations (from adjacent pipes) and an orifice equation that describes the leak. The orifice equation has a following form:

$$Q_L = C_d A_0 \sqrt{2gH_L} \tag{4.27}$$

where: Q_L = flow through the orifice
C_d = orifice discharge coefficient
A_0 = cross-section area of the orifice
H_L = hydraulic head at the leak

The continuity of mass must be applied for the node with a leak. A mass-balance equation represents the sum of the flows entering (positive) and exiting

(negative) the node. This sum is equal to zero:

$$Q_u - Q_d - Q_L = 0 \tag{4.28}$$

where Q_u and Q_d are the upstream and downstream flows, respectively, and are derived from the compatibility equations

$$C^+ \quad : \qquad Q_u = \frac{C_{P,u} - H_L}{B_u} \tag{4.29}$$

$$C^- \quad : \qquad Q_d = \frac{H_L - C_{M,d}}{B_d} \tag{4.30}$$

By substituting the orifice equation and the compatibility equations into Equation 4.28, the hydraulic head can be determined using a quadratic formula

$$H_i = a - b\sqrt{H_i} \tag{4.31}$$

$$\text{where:} \quad a = \frac{C_P B_M + C_M B_P}{B_M + B_P}$$

$$b = C_d A_0 \sqrt{2g} \frac{B_P B_M}{B_P + B_M}$$

After the head at the leaking node is obtained, flows Q_u and Q_d can be calculated from Equations 4.29 and 4.30, respectively.

In Equation 4.27, the leak is defined by the cross-sectional area of the orifice, A_0, and the discharge coefficient C_d. The value of C_d depends on the geometrical shape of the orifice. In practise, a lumped leak coefficient $C_d A_0$ is often used to define the leak size.

4.7 Burst boundary

The burst is simulated at the nodal points of the characteristic grid. The head and flow values at the burst point are calculated using the same expressions as those used for the leak case (Equation 4.31). The burst has the same discharge characteristics as the leak and the size of the burst is defined using the lumped

leak coefficient C_dA_0. The only difference between the burst and leak simulations is that the burst event itself (a burst opening) has to be simulated. In the case of a leak, C_dA_0 has a constant value during the simulation. However, the burst opening is simulated using a variable lumped leak coefficient. Before the burst has occurred, C_dA_0 is equal to zero. After the burst opening C_dA_0 is proportional to the defined size of the burst. Since it is not realistic that the burst reaches its defined size instantly, C_dA_0 cannot be changed from zero to the defined value within one time step of MOC solver. To simulate a longer burst opening, the leak coefficient is increased linearly from zero to the final value over a certain period of time. This time is equal to the defined burst opening duration. Such an implementation allows the simulation of bursts with different opening times.

4.8 Solving transients in pipe networks

The Method of Characteristics can be used to simulate transients in the pipe networks. When the system contains more than one pipeline, the interior sections of each pipeline are treated independently of other parts in the system at each instant in time. The end conditions for each pipe must interface with adjoining pipes or with other boundary elements. The elements around the node, having characteristic length Δx, are called computational units. Head and flow variables are allocated to computational units. Three types of variable allocation are illustrated in Figure 4.5. The choice of variable allocation type depends on the problem to be solved. For networks containing leakage, losses at junctions or valves, variable allocation type 3 is applicable.

The explicit MOC solution at a junction is demonstrated using the example junction (Figure 4.6) consisting of three pipes (or computational units). The positive x-direction for pipes 1 and 2 is defined into the junction and the positive x-direction for pipe 3 is defined out of the junction.

Two conditions are applied – the continuity of flows at the junction and the common hydraulic head at the junction. The characteristic equations are used to obtain the values for the head at the junction and flows in each of the pipes.

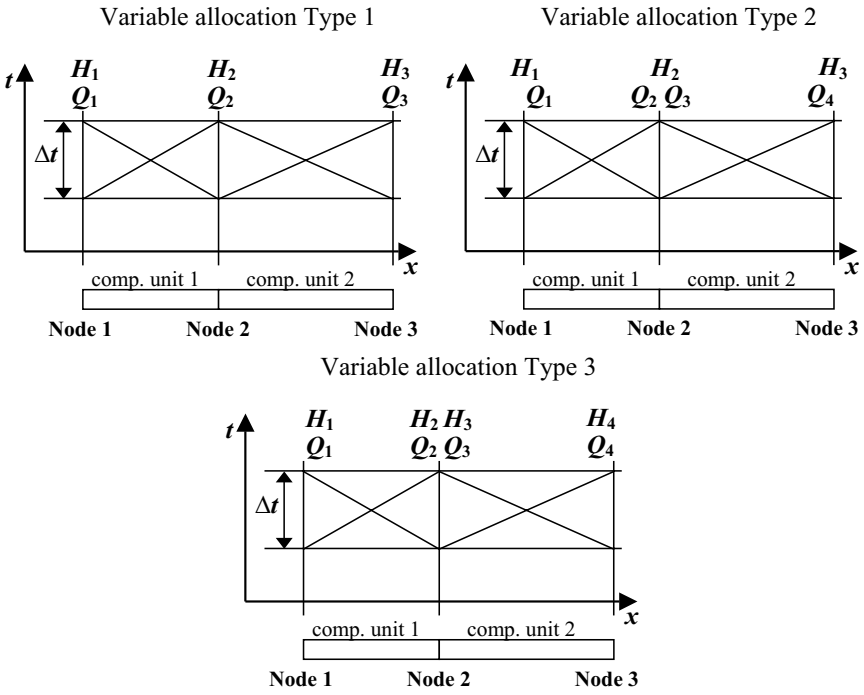

Figure 4.5: Computational units - variable allocation types.

A continuity equation at the junction is

$$\sum Q_P = Q_{P,1} + Q_{P,2} - Q_{P,3} = 0 \tag{4.32}$$

where flows entering the junction are positive and flows exiting the junction are negative. The compatibility equation for each pipe can be written in the following form:

$$Q_{P,1} = \frac{C_{P,1} - H_P}{B_1} \tag{4.33}$$

$$Q_{P,2} = \frac{C_{P,2} - H_P}{B_2} \tag{4.34}$$

$$Q_{P,3} = \frac{C_{M,3} - H_P}{B_3} \tag{4.35}$$

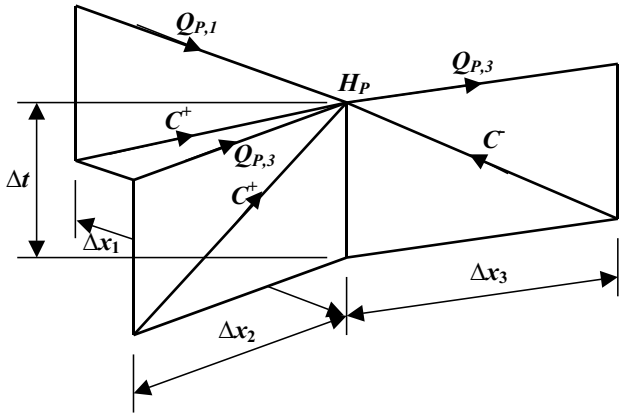

Figure 4.6: Characteristic lines at a junction.

Substituting the compatibility equations into continuity equation (Equation 4.32) gives the solution for the common head

$$H_P = \frac{\frac{C_{P,1}}{B_1} + \frac{C_{P,2}}{B_2} + \frac{C_{M,3}}{B_3}}{\frac{1}{B_1} + \frac{1}{B_2} + \frac{1}{B_3}} \tag{4.36}$$

The flows can be determined from Equations 4.33-4.35.

4.9 The choice of time step value

Determination of the adequate time step value for hydraulic transient simulation is an important procedure. A compromise between computational speed and accuracy has to be reached. Too small time step can require excessive computation, without any significant improvement, compared to the optimal one. Too great time step can mislead the interpretation of the results.

Limits of time step value

Computational time for simulation is a major factor that has to be considered when setting a lower limit for time step value. Every computer application includes certain limitations in terms of dynamic and static memory, which implies that the simulation time can be extensive, especially considering applications where a great number of repetitions is required. The simulation time is proportional to the total number of iterations that have to be carried out. The total number of iterations depends on the number of computation points in the system and the number of time steps in the simulation. The number of computational points is calculated from

$$N_{total} = \sum_{i=1}^{i=np} N_i \tag{4.37}$$

where np is the number of pipes in the network. If T_s is the duration of the physical process that has to be simulated, the number of iterations that have to be carried out in the simulation is equal to $T_s/\Delta t$ multiplied by N_{total}. Based on the maximum acceptable number of iterations the lower limit of the time step value, Δt_{min}, is chosen. However, numerical implementation of the MOC algorithm introduces additional restrictions on time step value selection. These restrictions are discussed in the following subsection.

Time step in MOC

The challenge of selecting a suitable time step arises from the nature of MOC. There are two conflicting constrains that have to be fulfilled: (1) if the system of two or more pipes is simulated, it is necessary that the time increment is equal for all pipes; (2) The Courant's criterion has to be satisfied for each pipe in the system (Wylie and Streeter; 1993):

$$\Delta t \leq \frac{\Delta x_i}{a_i}, \qquad i = 1,\ np \tag{4.38}$$

Ideally, the ratio of the space step Δx and the time step Δt must be equal to the wave speed a and the Courant number $C_r = a\Delta t/\Delta x$ must be equal to

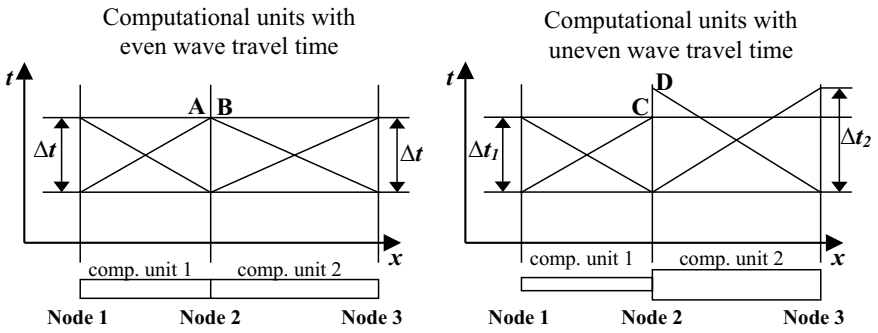

Figure 4.7: Characteristics lines for adjacent computational units with even and uneven wave travel times.

one. Thus, the optimal time step value for a pipe can be determined as follows:

$$\Delta t_i = \frac{L_i}{a_i N_i} \tag{4.39}$$

where L_i is the pipe length. When a diamond grid of MOC is implemented, the number of sections in the ith pipe N_i must be an even integer. The smallest even integer is 2. Thus, as suggested in Vugdelija et al. (2000), the Courant's criterion for a particular pipe can be defined as:

$$\Delta t \leq \frac{L_i}{2a_i}, \qquad i = 1,\ np \tag{4.40}$$

Both the length and the wave speed are the individual characteristics of a pipe. Thus, for a network transient simulation, the upper time step limit is:

$$\Delta t \leq min\left(\frac{L_i}{2a_i}\right), \qquad i = 1,\ np \tag{4.41}$$

To have a common time step value for all pipes and to satisfy a Courant's criterion, the wave travel time $a\Delta x$ has to be the same for a computational unit in any pipe of the network. This is almost impossible in a real network. Different pipe lengths and wave speeds usually cause different wave travel times. Additionally, as already mentioned, the condition that the number of sections in the ith pipe, N_i, is an even integer needs to be satisfied for MOC. In general, any

value of Δt is likely to produce a different non-integer value of N_i for each of the pipes. Thus, N_i has to be rounded to the closest even integer:

$$N_i = 2\ int\left(\frac{L_i}{2a_i\Delta t}\right), \qquad i = 1,\ np \tag{4.42}$$

Figure 4.7 shows the characteristics lines for two adjacent computation units with equal and unequal wave travel times. In the case of an uneven wave travel time (right plot in Figure 4.7), the ends of the two characteristics lines do not meet at the same time. In order to solve the compatibility equations, an interpolation between points C and D must be introduced. Two alternatives for this can be found in the literature. The first possibility is to adjust one of the pipe properties (usually the wave speed), forcing the number of reaches to be an even integer and making the Courant number equal to one. The second way is to allow Courant number to be less than one and to interpolate between known grid points.

Interpolation

In this section the three most common interpolation schemes are presented and briefly discussed.

Spaceline and timeline interpolation

Both spaceline and timeline interpolation schemes (see Figure 4.8) use interpolation between grid points to obtain values of the dependent variables at the foot of the characteristics lines. Since the physical parameters of the system and the values of the dependent variables at the adjacent nodes are known, it seems to be a simple matter to produce a good estimate. However, as noted in Ghidaoui et al. (1998); Greco and Carravetta (1999); Karney and Ghidaoui (1997), the function value at the foot of the characteristics can seldom be determined with certainty using this interpolation procedure. It is therefore suggested that the wave speed adjustment approach be used if the required wave speed correction is smaller than a certain value, e.g. 15%.

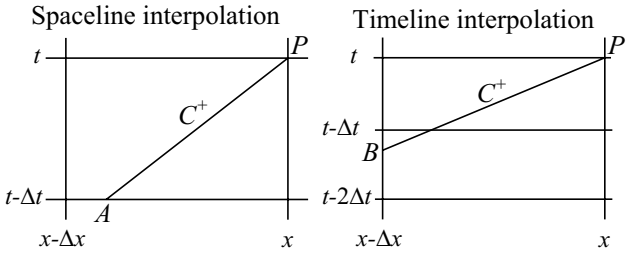

Figure 4.8: Spaceline (left) and timeline (right) interpolation schemes.

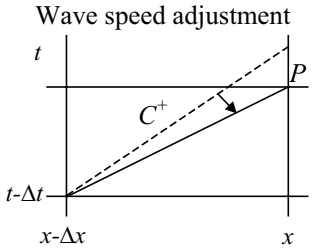

Figure 4.9: Wave speed adjustment.

Wave speed adjustment

The wave speed adjustment interpolation scheme (see Figure 4.9) is based on the adjustment of the wave speed values to equalise the numerical wave travel times of adjacent computational units. According to Ghidaoui et al. (1998), there are three main advantages of the wave speed adjustment over spaceline and timeline interpolation: (1) it preserves the physical shape of the wave; (2) it is partly justified by the uncertainty associated with wave celerity; and (3) the proportional change in wave speed is smaller than the associated degree of interpolation required by the previous interpolation schemes. Despite that, large wave speed adjustment modifies the wave travel time and distorts the timing of wave interactions. This drawback can be crucial for particular transient model applications, such as leakage detection. As proposed in Wylie and Streeter (1993) and Stapers (2002), the error introduced by the round-up of N_i

can be compensated by the correction of the wave speed a_i:

$$\Delta t = \frac{L_i}{a_i(1 \pm \psi_i)N_i} \tag{4.43}$$

Least squares approximation can be used to determine Δt such that the sum of squares of the wave speed adjustments ψ_i is minimal. Equation 4.43 can be rewritten as:

$$y = \begin{pmatrix} 1 \pm \psi_1 \\ 1 \pm \psi_2 \\ \vdots \\ 1 \pm \psi_J \end{pmatrix} = \begin{pmatrix} \frac{L_1}{a_1 N_1} \\ \frac{L_2}{a_2 N_2} \\ \vdots \\ \frac{L_J}{a_J N_J} \end{pmatrix} \left(\frac{1}{\Delta t}\right) = \Phi\Theta \tag{4.44}$$

where J is the total number of pipes in the network. An error vector is introduced as $e = y - y_m$, where y_m is a column vector $[J \times 1]$ of ones. The minimization of $\|\psi\|^2$ is achieved by solving the "normal" equation (Åström and Wittenmark; 1997):

$$\Theta = \left(\Phi^T \Phi\right)^{-1} \Phi^T y_m \tag{4.45}$$

The optimal Δt is given by $\Delta t = 1/\Theta$.

4.10 Unsteady friction

The traditional approach to incorporate frictional effects into the governing unsteady equations for pipe flow has been to approximate them with steady state friction relationships. Further research on the topic has shown that steady state approximations are only partially correct and that the non-uniform flow velocity profile plays an important role in the damping. The extra frictional dissipation caused by fluid acceleration is referred to as unsteady friction. A number of models for unsteady friction can be found in the literature. The unsteady friction implementation in the MOC scheme presented in this chapter is based on the Zielke's unsteady friction model (Zielke; 1968). The model uses

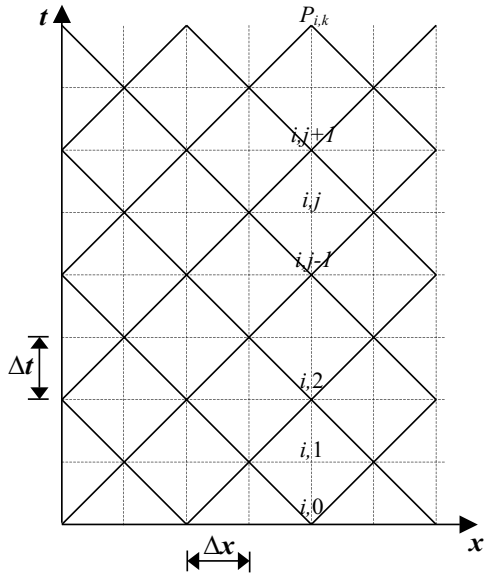

Figure 4.10: Grid of characteristics for specified time intervals.

weighted histories of past flows to determine the instantaneous shear stress. The expressions that describe laminar unsteady friction can be formulated for the MOC using a diamond grid. Figure 4.10 shows the grid with specified time intervals. The headloss at point $P_{i,k}$ can be expressed as the sum of steady and unsteady parts

$$h_{i,k} = \bar{h_{i,k}} + h'_{i,k} \tag{4.46}$$

$$\bar{h_{i,k}} = \frac{32\nu}{gD^2} V_{i,k} \tag{4.47}$$

$$\begin{aligned} h'_{i-k} = \frac{16\nu}{gD^2} &[(V_{i,k} - V_{i,k-2})W(\Delta t) + (V_{i,k-2} - V_{i,k-4})W(3\Delta t) \\ &+ \cdots + (V_{i,1} - V_{i,0})W((k-1)\Delta t)] \end{aligned} \tag{4.48}$$

where ν is the kinematic viscosity. The weight W is a function of the dimensionless time used to limit the influence of past velocity changes. The expression for calculating W is dependent on the flow regime defined by dimensionless

Reynolds number

$$Re = \frac{DV}{\nu} \tag{4.49}$$

Three different cases of flow regime are defined:

- Laminar smooth-walled flow. For the laminar flow:

$$Re < 2000 \tag{4.50}$$

- Turbulent smooth-walled flow:

$$Re > 2000 \tag{4.51}$$

- Fully rough-walled flow. The following relationship defines fully rough-walled flow:

$$Re > \frac{200D}{r\sqrt{f}} \tag{4.52}$$

  where r is the pipe roughness hight and f is a friction factor.

Laminar smooth-walled flow

The Zielke formulation (Zielke; 1968) is used to calculate the weighting function for laminar smooth-walled flow. The weights W are a function of the dimensionless time τ

$$\tau = \frac{\nu}{R^2}t \tag{4.53}$$

$W(\tau)$ approaches zero for $\tau \rightarrow \infty$ and can be calculated from the following series

$$\begin{aligned} \text{For } \tau &> 0.02 \\ W(\tau) &= e^{-26.3744\tau} + e^{-70.8493\tau} + e^{-135.0198\tau} + \\ &\quad e^{-218.9216\tau} + e^{-322.5544\tau} \end{aligned} \tag{4.54}$$

$$\begin{aligned} \text{For } \tau &\leq 0.02 \\ W(\tau) &= 0.282095\tau^{-\frac{1}{2}} - 1.250000 + 1.057855\tau^{\frac{1}{2}} + 0.937500\tau + \\ &\quad 0.396696\tau^{\frac{3}{2}} - 0.351563\tau^{2} \end{aligned} \tag{4.55}$$

Turbulent smooth-walled flow

For turbulent smooth-walled flow, the weighting function representation from Vardy and Brown (1996) is used, where

$$W(\tau) = \frac{A}{\sqrt{\tau}} e^{-\tau/C} \tag{4.56}$$

$$A = \frac{1}{2\sqrt{\pi}} \tag{4.57}$$

$$C = \frac{7.41}{Re^{\kappa}} \tag{4.58}$$

$$\kappa = \log_{10}(14.3/Re^{0.05}) \tag{4.59}$$

Fully rough-walled flow

In Vardy and Brown (2003), the model for the weighting function in a rough-walled pipe flow is derived as:

$$W(\tau) = \frac{A}{\sqrt{\tau}} e^{-\tau/C} \tag{4.60}$$

$$A = 0.0103\sqrt{Re}\left(\frac{r}{D}\right)^{0.39} \tag{4.61}$$

$$\frac{1}{C} = 0.352Re\left(\frac{r}{D}\right)^{0.41} \tag{4.62}$$

Once the appropriate weighting function value is calculated, the headloss at the characteristic point is derived from Equations 4.46 and 4.48.

4.11 Model validation

To validate the implemented transient flow model, a sudden valve closure experiment is used. The laboratory pipeline at The University of Adelaide, Australia (see Appendix A) was used to perform the experiment. A sudden valve closure at the downstream end of the pipeline was used to generate the transient. The simulation of the same scenario was made using the transient simulator described in this chapter. The comparison of simulated and measured data is

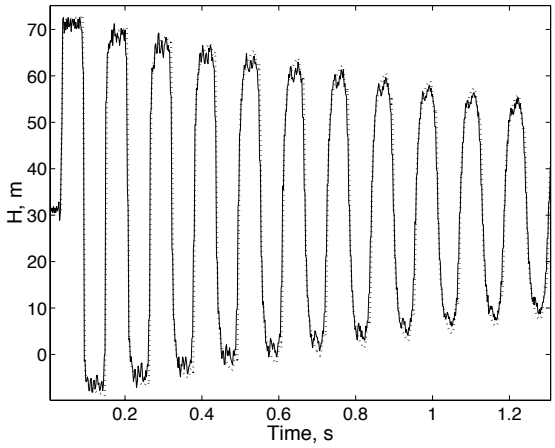

Figure 4.11: The measured (solid line) and simulated (dotted line) pressure traces.

shown in Figure 4.11. As can be seen from the figure, the discrepancy between simulated and measured pressure traces is minor.

Chapter 5

Burst detection and location in pipelines

In this chapter, a new technique for detecting and locating sudden bursts in pipelines is presented. The approach is based on continuous monitoring of pressure at one point along the pipeline and analysis of a burst-induced transient.

5.1 Introduction

As stated in Chapter 2, continuous monitoring of a pipeline is necessary for quick reaction to a burst event. Currently, there is no technique for continuous monitoring of water distribution pipelines. A number of different methods for pipe break detection have been applied in the gas and oil industries (see Chapter 3). Most of them combine continuous monitoring of the physical parameters with some form of mathematical model. There are two main parameters that are measured - pressure and flow. The number of measurement points varies from single point pressure monitoring (Schlattman; 1991; Whaley et al.; 1992) to pressure measurements at each end of the pipeline (Wang et al.; 1993) and even both pressure and flow measurements at each end of the pipeline (Emara-Shabaik et al.; 2002; Isermann; 1984; Liou and Tian; 1995; Mukherjee and Narasimhan; 1996; Zhang; 2001). Although the techniques using more meas-

urements have better performance, those applications require a great deal of instrumentation to be installed on the pipeline. The practical reality is that, opposite to the oil and gas industries where pipelines are already well instrumented and big investments can be made, water distribution mains are usually poorly instrumented and the budget of the water utilities does not allow for big investments. Therefore the techniques requiring the least amount of hardware installation are of the most interest. It is, however, essential that the location of the burst is found. The existing single-point pressure analysis approaches can only detect bursts, but not locate them.

The approach presented in this chapter is based on pressure transient analysis. The principles of time domain reflectometry (see Chapter 3) are adopted for detecting and locating abrupt pipeline bursts. The main idea is that the sudden burst initiates a pressure wave, which is later reflected from the boundaries. In Silva et al. (1996), it is shown that the burst location can be determined based on the wave arrival times observed at two (or more) measurement points. The algorithm presented in this chapter uses only one pressure measurement point to detect and locate the burst.

5.2 Burst location based on transient analysis

The location of a burst in a pipeline can be determined based on the timing of the burst-induced pressure transient wave reflections. When a burst occurs in a pipeline a negative pressure wave is generated and propagates in both directions away from the burst location. Eventually both waves reach the boundaries of the pipeline and are reflected. The timing of the reflections depends on the location of the burst. The travel times of the transient waves can be found using a pressure measurement sampled at a high frequency at one point along the pipeline.

The propagation of the burst-induced wave

An example pipeline system and principal transient pressure trace are shown in Figure 5.1. A burst occurs at point B and the pressure is measured at point M. Pressure variations at the measurement point M are caused by the burst-induced

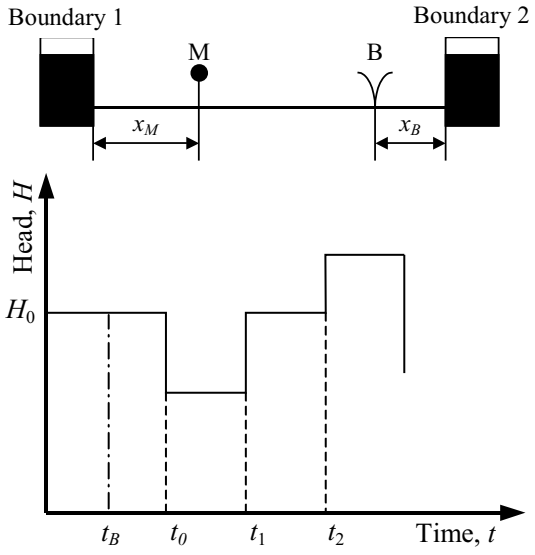

Figure 5.1: The example pipeline system and the generalised pipe burst transient trace measured at point M.

wave and its reflections from the pipeline boundaries. The propagation of the transient wave can be explained using the following time sequence:

$t < t_B$: Before the burst event the pressure along the pipeline is equal to the steady-state pressure H_0.

$t = t_B$: The burst event occurs at point B. A sudden increase in flow initiates a pressure transient at the burst point.

$t_B < t < t_0$: Two negative pressure waves are travelling in both directions away from the burst point B. The first wave propagates towards Boundary 1 and the second wave propagates towards Boundary 2.

$t = t_0$: The first wave reaches the measurement point M, which results in sudden decrease of measured pressure. Meanwhile, the second wave reaches Boundary 2 and is reflected.

$t_0 < t < t_1$: Both waves continue travelling along the pipeline. Eventually, the first wave is reflected from Boundary 1.

$t = t_1$: The reflection of the second wave from Boundary 2 reaches the measurement point M, which results in sudden change of measured pressure.

$t_1 < t < t_2$: The first wave, reflected from Boundary 1, approaches M.

$t = t_2$: The first wave reaches measurement point M, which results in sudden change of measured pressure.

The sequence of wave reflections continues in the same manner until the transient wave magnitude is equal to zero. The wave is damped due to the frictional effects. For the burst detection and location, the time interval $[t_B : t_2]$ is used.

The location of the burst

The sign and magnitude of transient pressure changes that take place at times t_0, t_1, and t_2 depend on the reflection characteristics of the boundaries in a particular pipeline. As already noted, the timing of the changes in the transient trace (t_0, t_1 and t_2) depends on the position of the burst. If the example trace in Figure 5.1 is considered, the position of the burst can be estimated from the time differences $\Delta t_1 = (t_1 - t_0)$ and $\Delta t_2 = (t_2 - t_0)$. If the distance from the burst to the closest boundary, x_B, is shorter than the distance from the measurement point to the closest boundary, x_M, the time difference Δt_1 will correspond to x_B. Δt_2 in this case will be proportional to the distance from the measurement point to the other boundary (not necessarily the closest one). Alternatively, if $x_B > x_M$, the time difference Δt_2 will correspond to x_B. Since x_M is known, the time difference associated with the position of the measurement point can be identified. Assuming that times t_0, t_1, and t_2 from Figure 5.1 are known, Δt_1, Δt_2 can be calculated. The times associated with the measurement point location with respect to both boundaries are derived from:

$$\begin{aligned} t_{M,1} &= \frac{2(L - x_M)}{a} \\ t_{M,2} &= \frac{2x_M}{a} \end{aligned} \tag{5.1}$$

where a is the wave speed of the pipe, $t_{M,1}$ is the time required for a transient wave to travel from the measurement point to boundary 1 and back, and $t_{M,2}$ is the time required for the transient wave to travel from the measurement point

to boundary 2 and back. The following rules can then be used to determine the burst position:

$$\begin{aligned}
&\text{if } \Delta t_1 = t_{M,1} \quad \text{then} \quad x_{B,2} = \frac{a\Delta t_2}{2} \\
&\text{if } \Delta t_1 = t_{M,2} \quad \text{then} \quad x_{B,1} = \frac{a\Delta t_2}{2} \\
&\text{if } \Delta t_2 = t_{M,1} \quad \text{then} \quad x_{B,2} = \frac{a\Delta t_1}{2} \\
&\text{if } \Delta t_2 = t_{M,2} \quad \text{then} \quad x_{B,1} = \frac{a\Delta t_1}{2}
\end{aligned} \tag{5.2}$$

where $x_{B,1}$ and $x_{B,2}$ are the distances from the burst point to boundary 1 and boundary 2, respectively. Since, in many cases, the precise value of the wave speed of the pipeline is not known, an error will be introduced when the burst position is calculated. To reduce this error, the wave speed can be eliminated. The rules in Equation 5.2 then become:

$$\begin{aligned}
&\text{if } \Delta t_1 = t_{M,1} \quad \text{then} \quad x_{B,2} = \frac{X_{M,1}\Delta t_2}{\Delta t_1} \\
&\text{if } \Delta t_1 = t_{M,2} \quad \text{then} \quad x_{B,1} = \frac{X_{M,2}\Delta t_2}{\Delta t_1} \\
&\text{if } \Delta t_2 = t_{M,1} \quad \text{then} \quad x_{B,2} = \frac{X_{M,1}\Delta t_1}{\Delta t_2} \\
&\text{if } \Delta t_2 = t_{M,2} \quad \text{then} \quad x_{B,1} = \frac{X_{M,2}\Delta t_1}{\Delta t_2}
\end{aligned} \tag{5.3}$$

The size of the burst

The approximate burst size can be calculated using Joukowsky pressure rise formula combined with the orifice equation (see Appendix C):

$$C_d A_0 = \frac{A|\Delta H|\sqrt{2g}}{a\sqrt{H_0 - \Delta H}} \tag{5.4}$$

where ΔH = head change due to the burst
H_0 = is initial system head
A = pipe cross-sectional area
$C_d A_0$ = lumped burst orifice parameter

After the burst position is determined using the rules in Equation 5.3 and the size of the burst is estimated from Equation 5.4, validation of the obtained parameters can be performed. A burst of the estimated size is simulated at the derived position using the transient solver (Chapter 4). If a good fit between the simulated and measured data is observed, the burst position and size can be confirmed.

5.3 Continuous burst monitoring approach

The proposed continuous burst monitoring algorithm is illustrated in Figure 5.2. The algorithm can be divided into two parts: (1) continuous monitoring of measured pressure for a burst event and (2) analysis of the data and estimation of burst parameters.

Monitoring for a burst event

The measured pressure trace is continuously monitored for a burst event. In case of a burst, a negative change in the measured pressure would occur. The cumulative sum (CUSUM) test (Basseville and Nikiforov; 1993; Page; 1954) is used to monitor the changes in the data. Since the pressure measurement from the real system can contain a considerable amount of noise, pre-filtering of the signal is carried out.The adaptive Recursive Least Squares (RLS) filter is used to reduce the noise content. The filter estimates the signal θ_t from the measurement y_t as:

$$\theta_t = \lambda\theta_{t-1} + (1-\lambda)\, y_t = \theta_{t-1} + (1-\lambda)\, \epsilon_t \tag{5.5}$$

where $\epsilon_t = y_t - \theta_{t-1}$ is the prediction error and the parameter $\lambda[0,1)$ is the forgetting factor. The filtered signal θ_t and the residuals are fed into the CUSUM algorithm to determine whether a change has occurred. Mathematically, the test is formulated as the following time recursion:

$$\begin{aligned} &g_0 = 0 \\ &g_t = \max\left(g_{t-1} - \epsilon_t - \nu, 0\right) \\ &\text{if } g_t > h \text{ then issue the alarm and set } t_a = t,\ g_t = 0 \end{aligned} \tag{5.6}$$

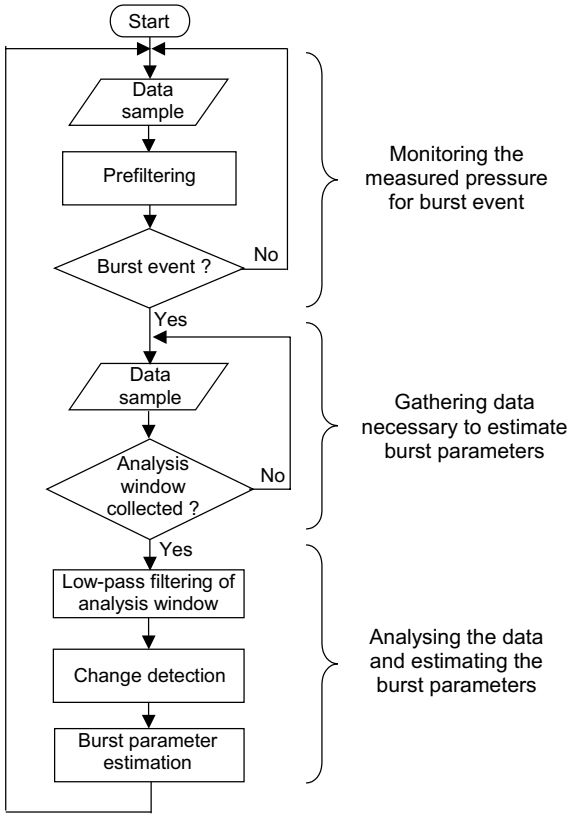

Figure 5.2: The structure of continuous burst monitoring algorithm.

where h and ν are threshold and drift parameters, respectively. The threshold limits the size of the burst that will be detected. A smaller value of the threshold will result in the detection of smaller bursts. Since the magnitude of the change is proportional to the size of the burst and not known in advance, the minimal size of the burst that will be detected is selected. The threshold h is set to be equal to the pressure change ΔH_{min}, which corresponds to the minimal size of the burst and can be derived from Equation 5.4 as:

$$\Delta H_{min} = \frac{C_d A_0 a \sqrt{H_0}}{A\sqrt{2g}} \tag{5.7}$$

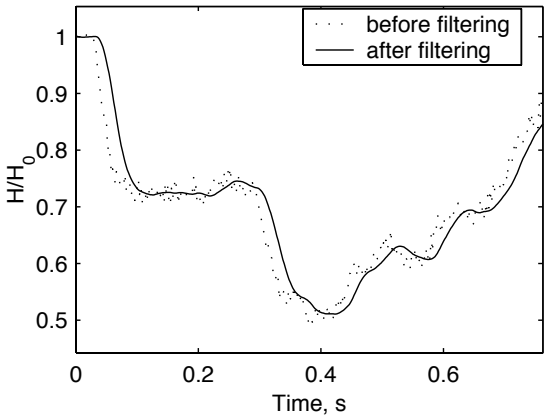

Figure 5.3: An example of an analysis window and the effect of filtering.

The drift ν is chosen so that only changes exceeding the steady state noise bandwidth are taken into account.

Analysis window

Once a negative change in measured pressure is detected and the time of change t_a is set, the second part of the algorithm is started. The analysis window of the data is selected. The size of the window is proportional to the maximum distance from the measurement point to the two boundaries:

$$T_W = \frac{2 \max\left(x_{M,1}, x_{M,2}\right)}{a} \tag{5.8}$$

where T_W is the analysis window's length in time units. Once the data interval $[\, t_a : t_a + T_W]$ has been collected, off-line analysis is performed. In order to identify all changes in the data, including the one induced by the first arrival of the burst wave, a wider window is used by including a certain portion of data prior to t_a. Thus the interval $[\, t_a - T_\epsilon : t_a + T_W]$ is used. To remove the high frequency oscillations, the data is filtered using a second-order Butterworth low-pass filter. The cut-off frequency of the filter is chosen based on the characteristics of the noise in the data. An example of the analysis window and

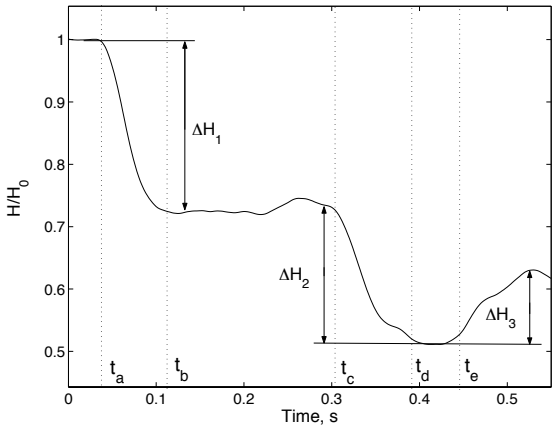

Figure 5.4: Division of the analysis window. Vertical lines indicate changes between states.

the effect of filtering are shown in Figure 5.3. As can be observed, the filtering introduces a certain delay in the data. However, this delay has no influence on the results of the burst detection and location technique; the burst position is proportional to the difference between time instances t_0, t_1 and t_2 (Figure 5.1) and not the absolute time.

Change detection

After filtering, analysis of the measured pressure data is performed. Three time instances (t_0, t_1 and t_2) have to be identified. These time instances correspond to the times t_a, t_c and t_e in the example pressure trace shown in Figure 5.4. The basic concept of the proposed algorithm for detecting changes in pressure data is taken from the CUSUM change detection test. Two states of the signal can be defined: (1) steady state and (2) transient state. In Figure 5.4 the steady state corresponds to the time intervals $[t < t_a]$, $[t_b < t < t_c]$ and $[t_d < t < t_e]$, whereas the transient state corresponds to the time intervals $[t_a < t < t_b]$ and $[t_c < t < t_d]$. The transitions from steady state to transient state are detected by means of the two-side CUSUM test (Equation 5.9). By using a two-side

test, both positive and negative changes in the measured signal are detected.

$$\begin{aligned} &g_0^1 = 0 \text{ and } g_0^2 = 0 \\ &g_t^1 = \max\left(g_{t-1}^1 - \epsilon_t - \nu, 0\right) \text{ and } g_t^2 = \max\left(g_{t-1}^2 - \epsilon_t - \nu, 0\right) \\ &\text{if } \left(g_t^1 > h \text{ or } g_t^2 > h\right) \text{ then issue the alarm and set} \\ &t_a = t,\ g_t^1 = g_t^2 = 0 \end{aligned} \tag{5.9}$$

The duration of the transient state is proportional to the burst opening time. When the variation of the measured signal becomes smaller than a certain predefined value, a new steady state is declared. The CUSUM change detection test is then reset for the detection of further changes.

Adaptive parameter tuning

For a better performance of the change detection algorithm, adaptive tuning of the threshold and drift parameters is implemented. The initial value of the threshold (h) is related to the minimum detectable burst size. This value is chosen in the first part of the algorithm. As the noise is filtered out from the pressure measurement, the initial drift value (ν) is no longer equal to the noise bandwidth of the filtered signal. The initial value of ν is set to 20% of h.

After the first change has occurred and the magnitude of the change is identified (ΔH_1 in Figure 5.4), the threshold and drift values are tuned. The threshold h is adjusted so that ΔH_2 and ΔH_3 (Figure 5.4) are detected and smaller variations are ignored. The new value of the threshold is set to:

$$h < \min\left(\Delta H_2, \Delta H_3\right) \tag{5.10}$$

where ΔH_2 and ΔH_3 correspond to the magnitudes of the burst-induced waves after reflection from the pipeline boundaries. The reflection characteristics of the boundaries are quantified by reflection coefficients that can be derived using the Method of Characteristics (see Appendix B). By multiplying the magnitude of the primary burst induced wave ΔH_1 by the reflection coefficients of the boundaries, ΔH_2 and ΔH_3 can be approximately calculated. Uncertainty is introduced by neglecting the frictional effects. Frictional damping of a particular pipeline has to be evaluated to make the best judgement about how small a

threshold values would work compared to the size of the change that has to be detected (Equation 5.10).

The drift ν is tuned to fit the opening time of the burst. This time is proportional to the slope of the pressure trace after the first change has occurred (interval $(t_a,\ t_b)$ in Figure 5.4). The slope can be characterised by the change in pressure dH that occurs during one sampling period dt. The drift value has to be smaller than dH for a change to be detected by the algorithm.

After the time differences Δt_1 and Δt_2 have been calculated, the burst position x_B is estimated according to the rules in Equation 5.3.

5.4 Laboratory validation

To validate the proposed technique under controlled conditions, the continuous monitoring approach for burst detection was tested in a laboratory pipeline (the laboratory pipeline was located at the School of Civil and Environmental Engineering at the University of Adelaide, Australia, for more details see Appendix A). The laboratory apparatus comprises a 37.527 m long 22.1 mm diameter copper pipeline (Bergant and Simpson; 1995). An initial flow in the pipeline is generated by a head difference between two computer-controlled pressurised tanks. The calibrated wave speed of the pipe is 1327 m/s. The burst was simulated using a fast-opening solenoid side discharge valve. The opening time of the solenoid valve is 4 ms. Additionally, a manual side discharge valve was used for simulating bursts with longer opening times. The setup was such that the entrance to both tanks were open, which is realistic when considering a real transmission pipeline. A $PDCR810$ Druck transducer was used to measure the pressure. The data acquisition was performed using Visual Designer software with a sampling rate of 2 kHz.

Five tests were carried out. Tests 1 to 4 considered a fast opening burst located at various positions along the pipeline. The burst was located at 0.1784, 0.4985, 0.7476, and 0.9936 (expressed as a fraction of the total pipeline length) along the pipeline for tests 1 to 4, respectively. The pressure was measured at 0.1784 along the pipeline. The calibrated size of the burst in each case was $C_d A_0 = 1.7665{\cdot}10^{-6}$ m^2. Since the noise level in the experimental data was low, no prefiltering was performed ($\lambda = 0$). The cut-off frequency of the Butterworth filter

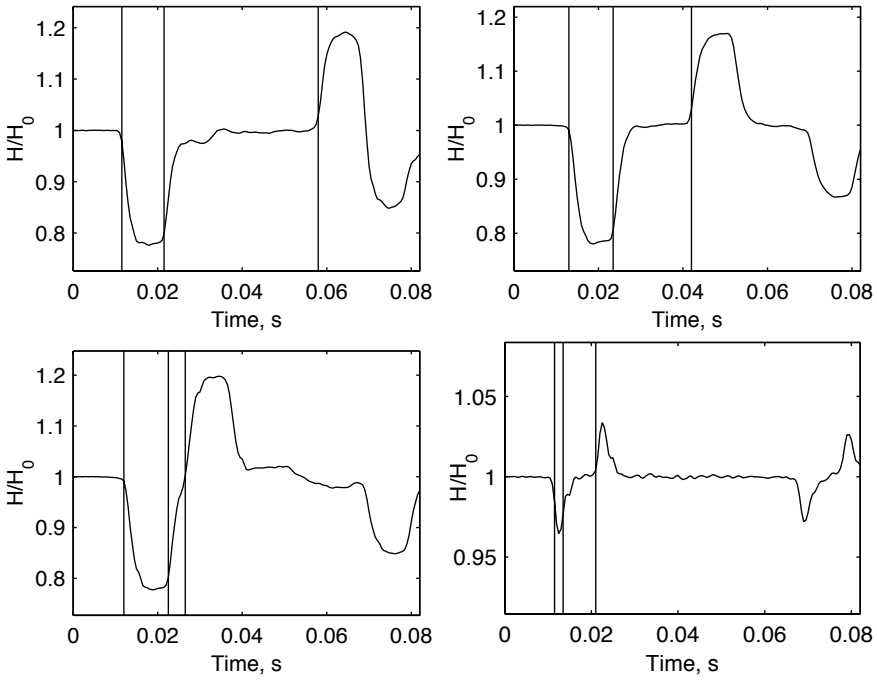

Figure 5.5: Pressure traces and detected changes (vertical lines) for tests $1-4$. The burst was located at 0.1784 (upper left), 0.4985 (upper right), 0.7476 (lower left) and test 0.9936 (lower right) along the pipeline. The pressure was measured at 0.1784 along the pipeline.

was set to 600 Hz and the diameter of the orifice of the minimum burst was set to 1% of the pipe diameter. The experimental pressure traces and detected changes for the four tests are shown in Figure 5.5. The numerical results can be found in Table 5.1.

In each test case, the burst was quickly and accurately located. However, the burst occurring in the vicinity of the right-hand tank (at a position of 0.9936) was less accurately located. A potential reason for this is explained later in this chapter. In cases 1, 2 and 3, the estimates of the burst orifice size are within 2% of the correct value. For test 4 the estimated burst orifice size is largely underestimated; again reasons for this are given later in the chapter.

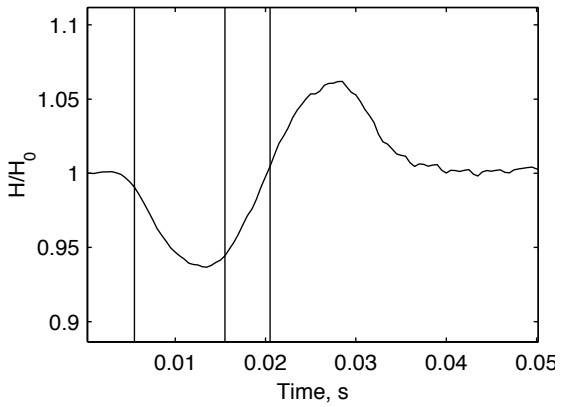

Figure 5.6: Pressure trace and detected changes for a slower burst located at 0.1784 along the pipeline. The pressure was measured at 0.7476 along the pipeline.

Test	Actual x_B Actual C_dA_0 (m^2)	Estimated x_B Estimated C_dA_0 (m^2)	Absolute error in x_B (m) Relative error in C_dA_0 (%)
1	0.1784 1.7665×10^{-6}	0.1767 1.7635×10^{-6}	0.0642m -0.1691%
2	0.4985 1.7665×10^{-6}	0.5073 1.7356×10^{-6}	0.3294m -1.7496%
3	0.7476 1.7665×10^{-6}	0.7536 1.7530×10^{-6}	0.2266m -0.7622%
4	0.9936 1.7665×10^{-6}	0.9624 2.7098×10^{-7}	1.1693m -84.66%
5	0.1784 6.0192×10^{-7}	0.1683 5.1955×10^{-7}	0.3802m -13.685%

Table 5.1: Summary of laboratory burst detection tests.

Test 5 assesses the effectiveness of the online burst detection method when the burst opening occurs over a greater time period. In this case, a manually actuated side discharge valve was used to generate the burst at a position of 0.1784 along the pipeline. The estimated opening time of the burst was 30 ms. The calibrated size of the burst orifice was $6.0192 \cdot 10^{-7}$ m^2. Pressure measurement was collected at a position of 0.7476 along the pipeline. The burst was detected successfully even though the wave front created by the burst was much slower (Figure 5.6). The numerical results are presented in Table 5.1.

5.5 Field validation

In this section, the validation of the proposed burst detection and location technique under controlled field conditions is described and the results are presented. A more detailed description of the experimental site and experiments can be found in Appendix A. The technique was tested on 356.53 m long 100 mm diameter pipe in a real water distribution network. The network is located in the township of Willunga, approximately 80km south of Adelaide, Australia. The pipe is a dead-end branch connected to the rest of the system by a tee-junction. A number of residential household connections are attached to the pipe section. The experimentally derived wave speed value was equal to 1150 m/s. Fire hydrant plugs were used as a connection points for the measurement and burst generation equipment. The burst was simulated using a 10 mm diameter solenoid side discharge valve. The calibrated size of the valve burst was $C_d A_0 = 5.4978 \times 10^{-5}\text{m}^2$. The pressure measurements were collected at a 500Hz sampling frequency. The locations of the bursts are expressed as the ratio between the distance from the dead-end of the pipe to the burst point and total length of the pipeline.

Eight tests were carried out. Four burst locations were tested: 0.1421, 0.3999, 0.4981 and 0.7991 along the pipeline. Two different measurement sites were used. The first was located at the dead-end of the pipe and the second was 0.3999 along the pipeline. The cut-off frequency of the Butterworth filter was set to 12.5 Hz and the diameter of the orifice of the minimum burst was set to 1% of the pipe diameter. To illustrate the effect of filtering, the pressure traces before and after filtering for tests 6, 7 (Figure 5.7) and tests 10, 11 (Figure 5.8) are shown. As can be observed, the high frequency content of the signal is filtered out.

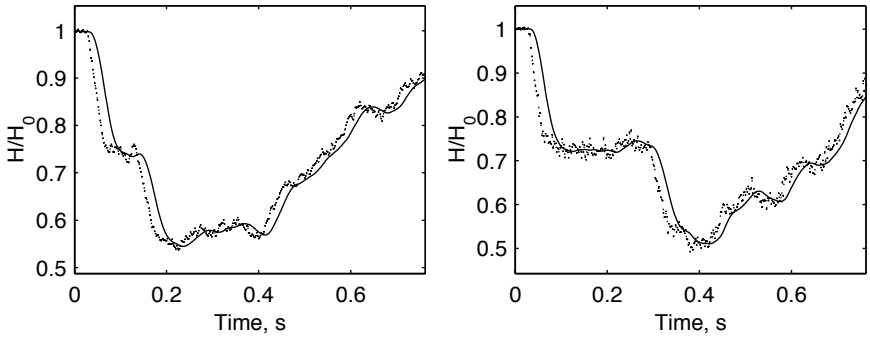

Figure 5.7: The analysis window and the effect of filtering for tests 6 (left) and 7 (right). The pressure was measured at the position of 0.3999 along pipeline.

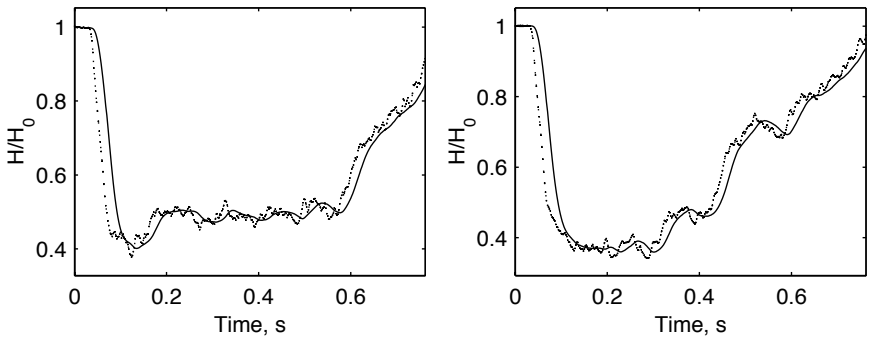

Figure 5.8: The analysis window and the effect of filtering for tests 10 (upper) and 11 (lower). The pressure was measured at the dead-end of the pipeline.

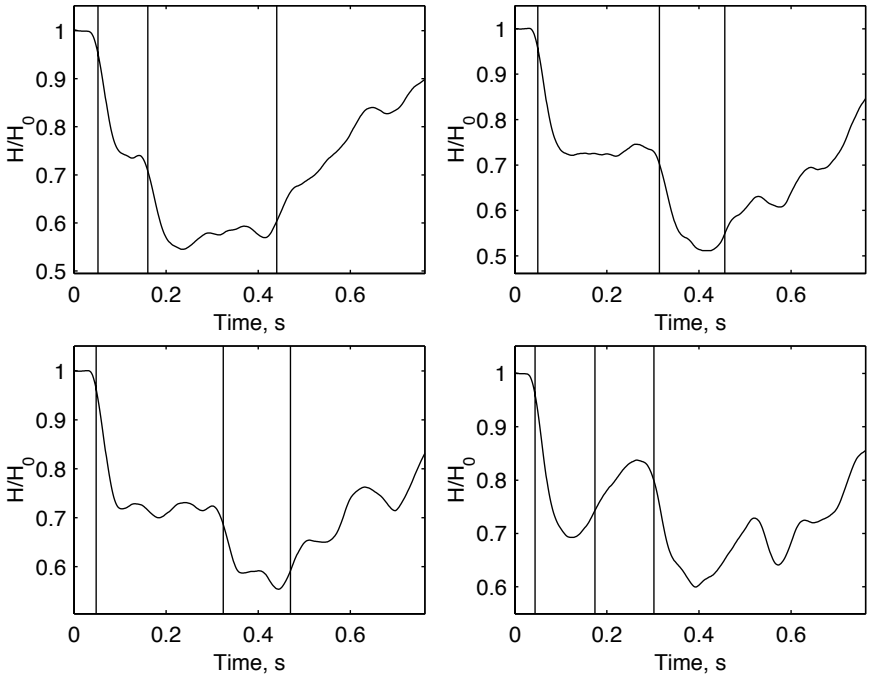

Figure 5.9: Pressure traces and detected changes (vertical lines) for tests $6-9$. The burst was located at 0.1421 (upper left), 0.3999 (upper right), 0.4981 (lower left) and 0.7991 (lower right) along the pipeline. The pressure was measured at the position of 0.3999 along the pipeline.

In Figure 5.9, the filtered pressure traces together with detected changes are shown for tests 6 to 9. The pressure was measured at 0.3999 along the pipeline. The corresponding plots for tests 10 to 13, where measurements were made at the dead-end of the pipeline, can be found in Figure 5.10.

The burst position and size are calculated from the results of the change detection routine and compared with the true values. The numerical results along with the corresponding errors for all the tests are summarised in Table 5.2.

All bursts are successfully detected. With the exception of the large error in the burst position for test 8, the errors in location and size of the burst are within reasonable limits. After further investigation of the pressure trace from test 8

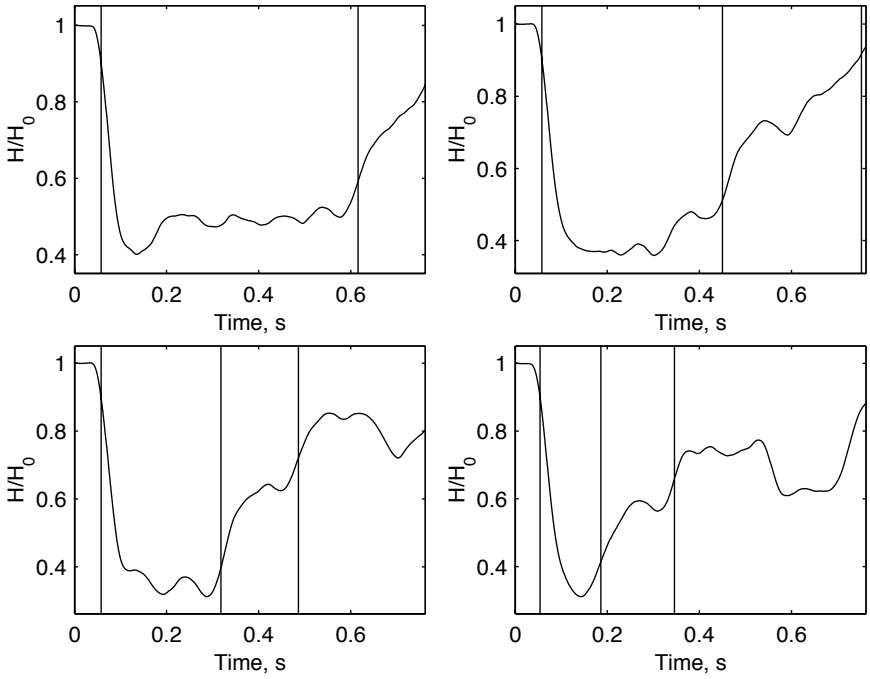

Figure 5.10: Pressure traces and detected changes (vertical lines) for tests $10-13$. The burst was located at 0.1421 (upper left), 0.3999 (upper right), 0.4981 (lower left) and 0.7991 (lower right) along the pipeline. The pressure was measured at the dead-end of the pipeline.

it appeared that the transient waves reflected from the boundaries arrived at the measurement point almost at the same time. The interaction of the waves occurred at the measurement point and the arrival times were not accurately captured in the pressure data. Results could be improved with an additional measurement point or a measurement point located elsewhere in the pipeline. As an example, test 12 can be considered where the burst was located in the same position as in test 8. In this case the pressure was measured at the dead-end of the pipe and the correct position of the burst was found.

Test	Actual x_B Actual C_dA_0 (m^2)	Estimated x_B Estimated C_dA_0 (m^2)	Absolute error in x_B (m) Relative error in C_dA_0 $(\%)$
6	0.1421 5.4978×10^{-5}	0.1670 5.1182×10^{-5}	8.8902m -6.9043%
7	0.3999 5.4978×10^{-5}	0.3850 5.3733×10^{-5}	5.3171m -2.264%
8	0.6013 5.4978×10^{-5}	0.3885 5.5841×10^{-5}	75.85m 1.5694%
9	0.7991 5.4978×10^{-5}	0.7985 5.8136×10^{-5}	0.2158m 5.7447%
10	0.1421 5.4978×10^{-5}	0.1000 4.7160×10^{-5}	14.9830m 14.2200%
11	0.3999 5.4978×10^{-5}	0.3678 5.4744×10^{-5}	11.4460m -0.4256%
12	0.6013 5.4978×10^{-5}	0.5807 5.9784×10^{-5}	7.3515m 8.7417%
13	0.7991 5.4978×10^{-5}	0.7871 6.0740×10^{-5}	4.2731m 10.48%

Table 5.2: Summary of field burst detection tests.

5.6 Considerations

There are a number of considerations that remain for the continuous monitoring technique for burst detection and location. Some are discussed in this section: (1) occurrence of bursts near boundaries, (2) the speed of burst opening, (3) measurement location, and (4) transients caused by normal pipeline operation.

Bursts near boundary

When a burst occurs near the boundary (test 4 in Section 5.4), the burst size estimate contains a large error. This is caused by the interaction of a burst-induced wave with the boundary before the burst has fully opened. In particular, as the burst begins to open, a negative pressure wave is generated that propagates away from the burst. If nothing interacts with the burst while it is opening, full pressure decrease is realised. However, if the burst is located near a boundary (like a

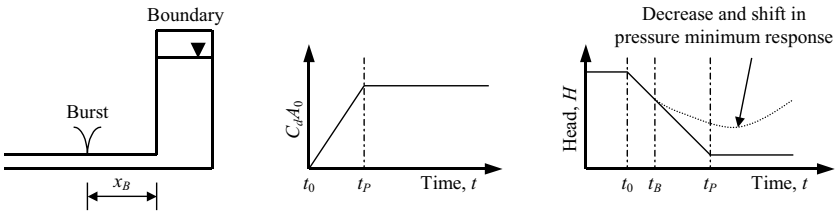

(a) Burst near boundary (b) Burst opening profile (c) Head response at burst

Figure 5.11: The occurrence of a burst near a pipeline boundary.

reservoir) so that the initial negative pressure wave is reflected off the boundary and arrives back at the burst before the burst has fully opened then the full pressure decrease is not realised. This effect is shown in Figure 5.11 where the burst is located at distance x_B from the boundary. The reflection time t_r is equal to

$$t_r = \frac{2x_B}{a} \tag{5.11}$$

If the burst opening time t_P is greater than t_r then some interaction will occur. An alternative way to explain the relation in Equation 5.11 is that the correct size of the burst will not be determined if the distance from the leak to the boundary is

$$x_B < \frac{t_P a}{2} \tag{5.12}$$

The speed of burst opening

In test 5 (Section 5.4), the technique was tested for a burst with longer opening time. As can be observed in the results, changes in the pressure data are detected with a certain delay. This delay is the same for all consecutive changes. Since the time differences between changes in the measurement are used to estimate the burst position, the delay has no influence on the performance of the burst location technique. When the burst opening time is longer than the wave travel time from the burst to the closest boundary and back, the burst wave starts interacting with the burst before the burst is fully open. This phenomenon has already been described earlier in this section. From Equation 5.12, it can be seen

that increasing the burst opening time will have the same effect on the results as decreasing the distance from the burst to the boundary. Thus, the conclusion can be made that the technique is effective only for quick burst events with opening time $t_P < 2x_B/a$. Here x_B is the distance from the burst point to the closest boundary.

The choice of measurement position

The choice of the measurement position is another important issue that can be a source of error in the burst position estimation. An example of such an error was demonstrated in test 8 (Section 5.5). The problem arises when the waves reflected from the boundaries reach the measurement point at the same (or almost the same) time. In such a situation, the waves interact and it is not possible to identify their exact arrival times at the measurement site. This causes an error in the burst position estimate. As shown in test 12, when the measurement is made at another position, the correct location of the burst is found. Thus, a separate analysis has to be performed to find a measurement position that would minimise the probability of such an error. Another potential problem is taking pressure measurements at the centre of the pipeline when both boundaries have the same reflection characteristics. In this case the arrival of the pressure reflections coincide, making determination of the true burst location difficult. This problem can be avoided by measuring at positions other than the centre of the pipeline.

Transients caused by normal operation

Finally, the pressure transients caused by the normal operation of the system also have to be taken into consideration. Pump startup and shutdown or valve operation are potential sources of false alarms. One way to deal with this problem is to temporarily disable the burst detection system for the duration of these events. Another option is to model the expected transient from the system operation and compare it with the measured one. The discrepancy between predicted and actual pressure traces would indicate a burst event.

Chapter 6

Burst detection and location in pipe networks

In this chapter, an approach for sudden burst detection and location in small scale pipe networks is presented. The proposed technique is based on burst-induced transient analysis.

6.1 Introduction

As opposed to the burst detection in pipelines, where a number of techniques have been developed for oil and gas applications, burst detection in pipe networks is still a poorly developed area. At present, there does not appear to be a comprehensive method for rapid detection and location of pipe breaks in water distribution networks. The DMA approach described in Chapter 3 has a long response time and does not locate the burst point. As indicated in Chapter 2, a quick response of the burst detection and location system can only be achieved by continuous monitoring.

The main ideas from the pipeline burst detection and location approach presented in Chapter 5 are translated for a network situation. A pipe network can be treated as a collection of single pipelines. In principle, it is possible to apply the burst detection and location technique described in Chapter 5 for each of these

pipelines separately. In reality, such a system would be infeasible due to the cost of installation. As already mentioned, the least investment demanding techniques are of most interest for the water industry. Therefore, a new approach is derived for burst detection and location in pipe networks.

The pressure is continuously monitored at two or more points throughout the network. A sudden burst induces a negative transient pressure wave. Eventually, a transient wave reaches the measurement points. Using the difference in wave arrival times at two measurement points, the burst location can be derived.

6.2 Burst location based on transient analysis

The negative pressure wave created by the burst travels in both directions away from the burst origin. It is reflected at the pipe junctions and boundaries. Assuming that the pressure is continuously measured at two points in the system, the time when the burst-induced wave reaches the measurement points can be used to detect and locate the burst. The magnitude of the wave at the measurement points can also be extracted from the data. These ideas form the basis of the proposed technique.

The timing of the transient wave

Generalised pressure traces at two measurement points for a burst-affected system are shown in Figure 6.1. The burst occurs at time t_B, which initially is not known. If the pressure is measured at nodes j and k, the travel times from the burst origin to the measurement sites $t_j - t_B$ and $t_k - t_B$ cannot be determined. However, since the measurements are synchronised, the difference between the arrival times $t_j - t_k$ is known. It is likely that this difference is unique for bursts occurring at different points in the network. The corresponding time difference can be calculated for all nodes in the system. Assuming that pipe parameters and wave speeds are known, it is possible to calculate the shortest wave travel time between any two points in the system. The wave travel time for a single pipe is equal to

$$\tau_p = \frac{L_p}{a_p} \tag{6.1}$$

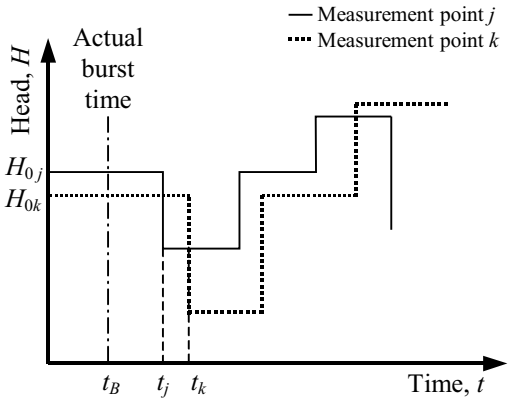

Figure 6.1: Generalised burst-affected transient traces.

where L_p is the length of the pipe and a_p is the wave speed of the pipe. One or more pipes connect any two nodes i and j in the network. The travel time between those nodes $\tau_{i,j}$ is the sum of the wave travel time τ_p of all pipes connecting them. In the case where alternative routes between nodes exist, the route with the shortest travel time is selected. As τ depends on both length and wave speed (Equation 6.1), the route having a shortest travel time does not necessarily correspond to the shortest distance between the nodes. The wave speed values can vary considerably for different pipe materials and roughness.

Once the travel times $\tau_{i,j}$ and $\tau_{i,k}$ are determined for a specific network of interest, the arrival time differences $\tau_{i,j} - \tau_{i,k}$ can be calculated. If the burst occurs at node i, where $i = 1, \ldots, N$ (the number of nodes in the network), the following equation should hold

$$(t_j - t_k) - (\tau_{i,j} - \tau_{i,k}) = 0 \tag{6.2}$$

Thus the burst location can be back-calculated using the measured time difference of the burst-induced wave and Equation 6.2.

The magnitude of the transient wave

The negative pressure wave initiated by the burst travels in both directions away from the burst point. It passes a number of pipe junctions before it reaches the measurement points and interacts with each of them. A certain portion of the wave is reflected at each junction, while the rest is transmitted. Since the route between nodes i and j, corresponding to the shortest travel time $\tau_{i,j}$, is known for a particular network, the wave transmission coefficient $T_{i,j} = \Delta H_j / \Delta H_i$ can be calculated. ΔH_i and ΔH_j are transient wave magnitudes at nodes i and j respectively. $T_{i,j}$ is the multiplication of transmission coefficients at every junction that the wave has to pass while travelling from node i to node j. Using the analysis of Wylie (1983), the wave transmission coefficient T_n can be derived (see Appendix B). For a general junction n, connecting P pipes, in the case when the wave is approaching from pipe 1, T_n is equal to

$$T_n = \frac{(H_J - H_0)}{(H_W - H_0)} = \frac{\dfrac{2A_1}{a_1}}{\displaystyle\sum_{k=1}^{P} \frac{A_k}{a_k}} \tag{6.3}$$

where H_0 is the initial head at the junction, H_J is the head at the junction after the wave has interacted with it, and H_W is the magnitude of the initial wave. A_i is the cross-sectional area of the pipe. Additionally, the friction in the pipes will also affect the transmission coefficients (compare with the treatment of junctions for the Method of Characteristics in Wylie and Streeter (1993), which includes steady friction). However, the effect of friction is small and is neglected in Equation 6.3. In the case when the burst occurs at node i, the following relation should be true

$$\frac{\Delta H_j}{\Delta H_k} = \frac{T_{i,j}}{T_{i,k}} \tag{6.4}$$

where ΔH_j and ΔH_k are pressure wave magnitudes registered at measurement nodes j and k, respectively. $T_{i,j}$ is the transmission coefficient for the wave travelling between nodes i and j and $T_{i,k}$ is the transmission coefficient for the wave travelling between nodes i and k. The left-hand-side of Equation 6.4 will be close, but not equal, to zero. This is due to the fact that the friction is

neglected in Equation 6.3 and the calculated T_j will be different from the actual one.

To estimate the size of a burst, the magnitude of the burst-induced pressure change at the burst location has to be known. It is back-calculated from Equation 6.4:

$$\Delta H_i = \Delta H_j \frac{1}{T_{i,j}} = \Delta H_k \frac{1}{T_{i,k}} \tag{6.5}$$

Once the head change ΔH_i is known, the approximate burst size can be calculated using the Joukowsky pressure rise formula combined with the orifice equation (see Appendix C).

$$C_d A_0 = \frac{A|\Delta H_i|\sqrt{2g}}{a\sqrt{H_B}} \tag{6.6}$$

where H_B is the head at the burst point after the burst has occurred ($H_B = H_0 - \Delta H_i$) and $C_d A_0$ is a lumped discharge parameter describing the size of the burst. Since friction at the junction and along the pipes is not considerred, Equation 6.6 will not provide the exact size of the burst due to neglecting of frictional effects. However, the objective of burst monitoring is to locate the burst and evaluate the severity of it, not to determine the exact size.

The search algorithm

To identify the burst location, a search is performed. The search algorithm is based on Equations 6.2 and 6.4. The search is divided into two parts: (1) searching for the burst at the nodes, (2) searching for the burst between nodes along the pipe.

Part 1 - searching for bursting node

In the first part of the search algorithm, it is assumed that the burst has occurred at the node. Every node in the network is checked by calculating its score function based on Equation 6.2:

$$s_{1i} = \left[(t_j - t_k) - (\tau_{i,j} - \tau_{i,k})\right]^2 \tag{6.7}$$

where s_{1i} can be referred to as the score for node i. The smaller s_{1i} is, the higher the probability that the burst has occurred at node i. If any node has a score equal to zero, the probability that it is the burst node is equal to one. Additionally, nodes are tested using the objective function based on Equation 6.4:

$$\min\{s_{2i}\} = \min\left\{\left(\frac{\Delta H_j}{\Delta H_k} = \frac{T_{i,j}}{T_{i,k}}\right)^2\right\} \tag{6.8}$$

Ideally, if the burst has occurred at node i, s_{2i} should be equal to zero. Since Equation 6.3 does not account for friction, s_{2i} will never be zero. If a node is found having s_{1i} equal to zero and minimal s_{2i}, it can be nominated as the burst position. Also, if there are two or more nodes having s_{1i} equal to zero, the one having the smallest s_{2i} is selected. When the burst does not occur at the node, all nodes will have $s_{1i} > 0$. In this case, the search for burst along the pipes is performed by the second part of the algorithm.

Part 2 - searching for bursting pipe

A new set of possible burst positions is obtained by placing them along the pipes. Since the scores s_{1i} for all the nodes are already available from the first part of the algorithm, the possible burst position along the pipe p connecting nodes n and m can be calculated as:

$$\begin{aligned} \dot{x_B} &= \frac{s_{1n}}{s_{1n} + s_{1m}} L_p = \\ &= \frac{\left[(t_j - t_k) - (\tau_{n,j} - \tau_{n,k})\right]^2}{\left[(t_j - t_k) - (\tau_{n,j} - \tau_{n,k})\right]^2 + \left[(t_j - t_k) - (\tau_{m,j} - \tau_{m,k})\right]^2} L_p \end{aligned} \tag{6.9}$$

where $\dot{x_B}$ is the distance from node n to the possible burst point and L_p is the length of pipe p. In this way, a new set of nodes along the pipes is created. The shortest travel times $\tau_{i,j}$ and $\tau_{i,k}$ and the wave transmission coefficients $T_{i,j}$ and $T_{i,k}$ are recalculated for the new node positions. These nodes are then tested using the following objective function

$$\begin{aligned} &\min\{S_i\} = \\ &= \min\left\{w_1\left[(t_j - t_k) - (\tau_{i,j} - \tau_{i,k})\right]^2 + w_2\left(\frac{\Delta H_j}{\Delta H_k} = \frac{T_{i,j}}{T_{i,k}}\right)^2\right\} \end{aligned} \tag{6.10}$$

where the weighting factors w_1 and w_2 are used to put emphasis on either the travel time or the reflection part of the objective function. The sum of w_1 and w_2 must be equal to 1. When the node i with optimal S_i is found, the location of the burst is set to $\dot{x_B}$.

6.3 The choice of measurement positions

The choice of measurement positions is an important issue having a great influence on the effectiveness of the algorithm. If a network has N nodes, there are $\frac{1}{2}(N^2 - N)$ different combinations of measurement node pairs j, k (given that j, k is the same as k, j). There are two parameters that are relevant to the choice of measurement nodes. These parameters are (1) the difference in pressure wave arrival times to the measurement sites j and k, and (2) the magnitude of the pressure wave that reaches measurement sites. If two or more nodes have the same $\tau_{i,j} - \tau_{i,k}$ for measurements placed at nodes j and k, the algorithm will not give a unique solution. This means j and k have to be selected so that the number of nodes having the same difference in arrival times $\tau_{i,j} - \tau_{i,k}$ is minimised. On the other hand, if a large portion of the wave is reflected on its way to the measurement point, it can be difficult to detect the change in pressure data. Therefore, the measurement points with the greatest $T_{i,j}$ and $T_{i,k}$ are most suitable. The choice of the measurement points is described by the following steps:

1. For all possible combinations of nodes j and k calculate $\tau_{i,j} - \tau_{i,k}$ for every node.

2. Find the number of equal arrival time differences for each combination of j and k.

3. Find j and k that has the smallest number of equal $\tau_{i,j} - \tau_{i,k}$. If several best combinations of j and k are found, proceed to step four, otherwise use j and k as optimal measurement positions.

4. For all combinations of j and k having the same number of equal arrival

time differences calculate

$$Tsum_{j,k} = \sum_{i=1}^{N} T_{i,j} \cdot T_{i,k} \tag{6.11}$$

where N is a number of nodes in the network.

5. Find j and k with the largest $Tsum_{j,k}$, which corresponds to the optimal measurement locations.

Two situations can be identified when several pairs of nodes will have the same $\tau_{i,j} - \tau_{i,k}$. The first is when the pipes have only similar discrete length values. The probability for that to be the case in a real network is rather low, since pipe lengths are usually randomly distributed. The second situation is when both shortest paths, which the burst-induced pressure wave takes towards the measurement points, start in the same direction from the burst point. The probability of such a situation depends on the topology and size of the network. In the case of numerous nodes having the same difference in arrival times, more measurement points may be necessary.

6.4 Online change detection in measured signal

A continuous pressure measurement is performed at the measurement sites. When a negative pressure wave initiated by the burst reaches a measurement point, it is essential to identify the arrival time and the magnitude of the wave. Therefore an algorithm is required that can automatically detect real-time change in the pressure measurement. The CUSUM change detection test used for on-line monitoring of measured data was described in Section 5.3. Depending on the noise content of the measured signal, filtering might be necessary (Equation 5.5). The choice of CUSUM parameters depends on the minimal size of the burst that will be detected. The magnitude of changes in pressure during normal operation has to be considered. Such variations can be caused by changes in demand, valve operation, etc. The change detection algorithm has to be tuned so that false alarms are avoided.

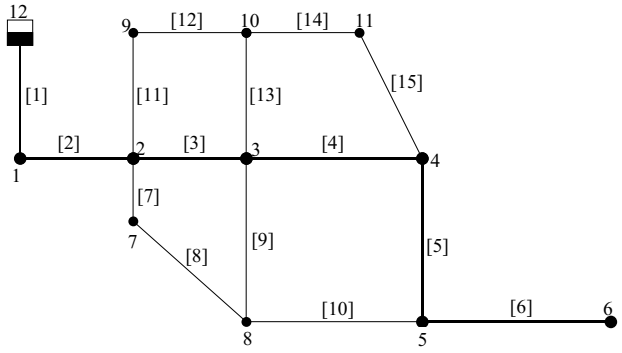

Figure 6.2: Layout of the network model.

6.5 Validation

The proposed technique was tested on an example network model. Burst simulations were used to obtain pressure data sets, which were later used as measured pressure traces. The layout of the network model is shown in Figure 6.2. It has 11 nodes, 15 pipes and is gravity-fed from a reservoir. The parameters of the pipes are shown in Table 6.1. The steady state head for all the nodes is 60m and there is no flow present. The burst was simulated as a rapidly opening discharge through an orifice with lumped parameter $C_d A_0 = 4.2239 \times 10^{-5}$ m^2. Burst opening time was set to 17ms. A forward transient solver as described in Chapter 4 was used to generate burst pressure traces.

The choice of the measurement positions was based on the algorithm explained in Section 6.3. First, steps 1 and 2 in the measurement node selection algorithm were applied. Two pairs of measurement nodes – $(6, 1)$ and $(9, 6)$ – had the minimal number of nodes with the same arrival time differences. After applying steps 4 and 5, nodes 9 and 6 were selected as measurement nodes. It is noted that two nodes, in particular nodes 1 and 2, had the same wave arrival time differences for the selected measurement locations. This means that in the case a burst occurs at one of these nodes a unique solution will not be obtained.

Two types of burst locations were tested: a burst occurring at a node and a burst occurring at some point along a pipe. For the first burst location type, 10 tests were carried out where bursts at different nodes were simulated. The simulated

Pipe No.	Length (m)	Diameter (mm)
1	120	300
2	140	300
3	200	300
4	220	300
5	180	300
6	280	300
7	100	100
8	220	100
9	240	100
10	200	100
11	220	100
12	140	100
13	220	100
14	160	100
15	280	100

Table 6.1: Parameters of the pipes. Wave speed for all pipes is 1200m/s.

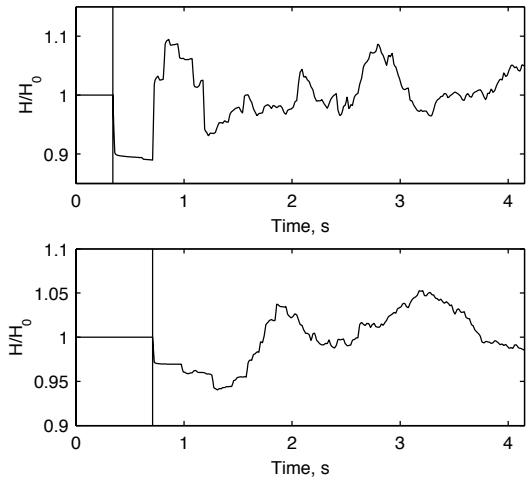

Figure 6.3: Test 9. Pressure traces at node 9 (upper) and node 6 (lower). Vertical lines illustrate changes detected by CUSUM algorithm. CUSUM parameters are $\nu = 0.01$, $h = 0.02$, $\lambda = 0$.

Test	Actual x_B Actual C_dA_0 (m^2)	Estimated x_B Estimated C_dA_0 (m^2)	Absolute error in x_B Relative error in C_dA_0
1	Node 2 4.2239×10^{-5}	Node 2 3.7946×10^{-5}	0 m -10.2%
2	Node 3 4.2239×10^{-5}	Node 3 3.8654×10^{-5}	0 m -8.5%
3	Node 4 4.2239×10^{-5}	Node 4 3.8253×10^{-5}	0 m -9.4%
4	Node 5 4.2239×10^{-5}	Node 5 3.7459×10^{-5}	0 m -11.3%
5	Node 7 4.2239×10^{-5}	Node 7 3.4642×10^{-5}	0 m -18.0%
6	Node 8 4.2239×10^{-5}	Node 8 1.4531×10^{-5}	0 m -18.3%
7	Node 9 4.2239×10^{-5}	Node 9 3.3753×10^{-5}	0 m -20.1%
8	Node 10 4.2239×10^{-5}	Node 10 3.5321×10^{-5}	0 m -16.3%
9	Node 11 4.2239×10^{-5}	Node 11 3.4934×10^{-5}	0 m -17.3%
10	Node 1 4.2239×10^{-5}	Node 1 3.4022×10^{-5}	0 m -19.5%

Table 6.2: Summary of results for tests $1 - 10$.

pressure data were used instead of real measurements. The pressure traces were tested using the change detection algorithm (see Equation 5.6 in Section 5.3). An example of change detection results (test 9) is shown in Figure 6.3. After the changes in pressure signals were detected, the search for burst position was performed. Once the location was found, the size of the burst was calculated from Equation 6.6. The results of the analysis for tests 1 to 10 are summarized in Table 6.2.

As observed, the algorithm was able to successfully locate bursts at all of the nodes with the exception of the situation when the burst occurred at node 1 (test 10). In this case, node 2 was identified as the location of the burst. This is due to the fact that the pressure wave initiated at node 1 travelled to both measurement points through node 2 and therefore $\tau_{1,9} - \tau_{1,6} = \tau_{2,9} - \tau_{2,6}$. Thus, both node 1 and node 2 had s_1 equal to zero (Equation 6.7). After applying Equation 6.8, node 2 had the smallest s_2 and was therefore selected as the burst position. The reason for node 2 having a smaller s_2 than node 1 is friction. The distances from node 1 to the measurement nodes are greater that the cor-

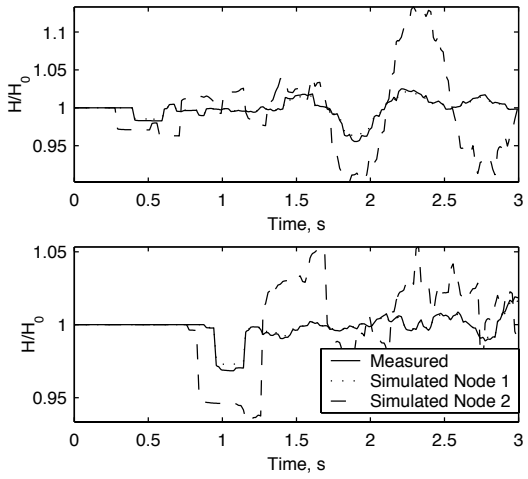

Figure 6.4: Comparison of measured and simulated pressure traces for test 10. Pressure at node 9 (upper) and node 6 (lower).

responding distances from node 2. Thus, the effect of the friction is larger when the wave is initiated at node 1. Since friction is neglected, s_2 for node 2 is smaller than s_2 for node 1. The fact that the ratio between ΔH_j and ΔH_k is the same for both cases suggests that, if the effect of friction would be known and precise wave transmission coefficients could be calculated, s_2 would be equal to zero for both nodes 1 and 2. In fact, this situation was identified previously when choosing the measurement locations. As was noted, if the burst occurs at nodes 1 or 2, a unique solution will not be found. This limitation is introduced by the topology of the network. Having an additional pressure measurement point would solve the problem. Importantly, the algorithm provides enough information to make one aware of such a situation. The actual burst position was found by comparing the measured pressure trace with results from burst simulations at nodes 1 and 2. Figure 6.4 shows the comparison of measured (solid line), simulated with burst at node 1 (dotted line), and simulated with burst at node 2 (dashed line) pressure traces. Simulating the burst at node 1 gives a much better fit to the measured data at both measurement points. Thus, the conclusion was that the burst occurred at node 1. The same check can be performed for test 1.

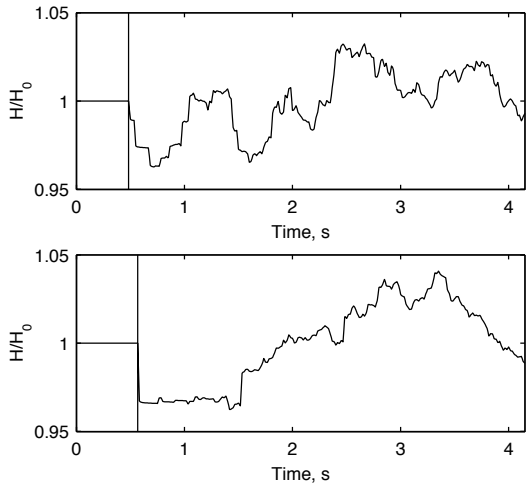

Figure 6.5: Test 12. Pressure traces at node 9 (upper) and node 6 (lower). Vertical lines illustrate changes detected by CUSUM algorithm. CUSUM parameters are $\nu = 0.01$, $h = 0.02$, $\lambda = 0$.

The burst sizes were estimated with a relative error of less than 21%. Even though the friction is neglected when estimating burst size, the precision of the estimate is sufficient for making conclusions about the severeness of the pipe fault.

For the case when the burst occurs at some point along the pipe, the performance of second part of the search algorithm was tested. 12 tests were carried out (test 11-22) where bursts at different locations along the pipes were simulated. Figure 6.5 illustrates the pressure traces at the measurement nodes for test 12. The vertical lines in the graph show the change times determined by the CUSUM change detection algorithm. The weights w_1 and w_2 in Equation 6.10 were set to 0.6 and 0.4 respectively. The detailed results of tests 11-22 can be found in Table 6.3.

The burst was successfully located at all locations with the largest relative position error being equal to 14.6% for test 11. The relative errors for remaining tests are significantly smaller. The burst size was estimated with a relative error of less than 19%.

Test	Actual x_B Actual C_dA_0 (m^2)	Estimated x_B Estimated C_dA_0 (m^2)	Absolute error in x_B Relative error in C_dA_0
11	Pipe 3, 90 m from Node 2 4.2239×10^{-5}	Pipe 3, 76.9 m from Node 2 3.9387×10^{-5}	13.1 m -6.8%
12	Pipe 4, 110 m from Node 3 4.2239×10^{-5}	Pipe 4, 110 m from Node 3 3.8966×10^{-5}	0 m -7.8%
13	Pipe 5, 80 m from Node 5 4.2239×10^{-5}	Pipe 5, 84.7 m from Node 4 3.8626×10^{-5}	4.7 m -8.6%
14	Pipe 6, 150 m from Node 5 4.2239×10^{-5}	Pipe 6, 150 m from Node 5 3.7528×10^{-5}	0 m -11.2%
15	Pipe 8, 110 m from Node 7 4.2239×10^{-5}	Pipe 8, 110 m from Node 7 3.4526×10^{-5}	0 m -18.5%
16	Pipe 9, 110 m from Node 3 4.2239×10^{-5}	Pipe 9, 113.7 m from Node 3 3.4229×10^{-5}	3.7 m -19%
17	Pipe 10, 90 m from Node 8 4.2239×10^{-5}	Pipe 10, 90 m from Node 8 3.4532×10^{-5}	0 m -18.3%
18	Pipe 11, 110 m from Node 2 4.2239×10^{-5}	Pipe 11, 110 m from Node 2 3.5049×10^{-5}	0 m -17%
19	Pipe 12, 70 m from Node 9 4.2239×10^{-5}	Pipe 12, 64.6 m from Node 9 3.5374×10^{-5}	0.6 m -16.3%
20	Pipe 13, 120 m from Node 3 4.2239×10^{-5}	Pipe 13, 120 m from Node 3 3.5577×10^{-5}	0 m -15.8%
21	Pipe 14, 70 m from Node 10 4.2239×10^{-5}	Pipe 14, 70 m from Node 10 3.4961×10^{-5}	0 m -17.2%
22	Pipe 15, 120 m from Node 11 4.2239×10^{-5}	Pipe 15, 120 m from Node 11 3.4890×10^{-5}	0 m -17.4%

Table 6.3: Summary of results for tests $11 - 22$.

Once the position and size of the burst were estimated, the results were verified by simulating the bursts with derived parameters. In Figure 6.6, the verification of the results from test 12 is presented. The two data series show a good fit, which suggests that the burst was located successfully. As expected, due to neglected frictional effects, there is a small discrepancy in the magnitude of the transients.

6.6 Limitations and considerations

There are a few issues that should be mentioned while considering the limitations of the proposed algorithm. First of all, in the case of a symmetric network, where some nodes have the same difference in wave arrival times $\tau_{i,j} - \tau_{i,k}$, a unique solution will not be found. This problem is described in Section 6.3.

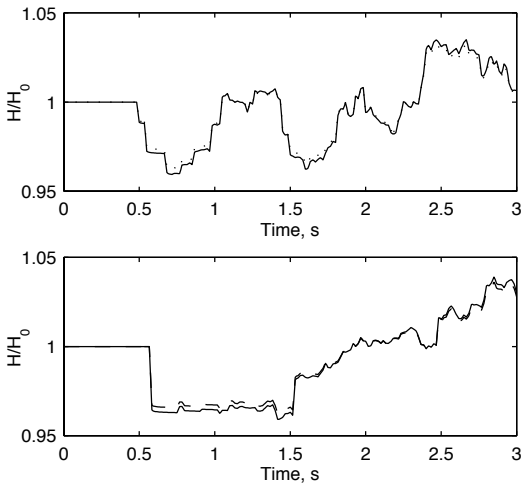

Figure 6.6: Verification of estimated burst position and size for test 12. Pressure traces at node 9 (upper) and node 6 (lower). Dotted line is transient trace for burst with estimated parameters.

In the case when pipes have similar discrete lengths, increasing the number of search points can solve the problem. In other words, more points throughout the network can be selected as "nodes". When some nodes have equal differences in wave arrival times because of the topology or size of the system, there are two ways to resolve the situation. If the number of "identical" nodes is small, simulation of the burst can be carried out. Simulating bursts at all nodes having the same $\tau_{i,j} - \tau_{i,k}$ and comparing the results with measured data will determine the actual location of the burst. If the number of "identical" nodes is large, one or few additional measurement points have to be added. The density of measurement sites should be proportional to the size of the network. It is obvious that in a larger system the burst-induced wave will interact with more junctions before it reaches the measurement points. This can lead to a situation where no change in measured pressure will be detected due to the damping of the burst-induced wave. Thus, more measurement sites, that are well distributed throughout the network, will be necessary.

Real pressure data contain a certain level of noise, which will decrease the preci-

sion of locating the burst. The lower precision is considered satisfactory as long as the broken pipe can be identified, rather than the exact location within the broken pipe. Once the pipe failure is detected and located, the next action is to isolate the burst by switching off that section of the network, i.e. the broken pipe. The precision of the burst location estimate is also dependent on the sampling frequency of the pressure measurement. A larger sampling interval will limit the precision of detected changes in the measured data, and, consequently, the precision of the burst location. Additionally, uncertainty with regard to the wave speed can cause errors in the results. Therefore the calculated wave speed values should be calibrated for the real system. The calibration can be performed by injecting sharp transients into the network and measuring wave travel times. Such a procedure is also useful for identifying abnormalities within the pipes (such as blocks, broken valves, etc.).

Finally, the transients caused by normal system operation have to be considered. Pump shutdowns or a sudden legitimate increase in demand can cause a pressure variation at the measurement site similar to that of a burst. Thus, estimated burst locations at (or close to) pumping stations or demand points should be treated with caution.

Chapter 7

Concluding remarks

The topic of this thesis is detection and location of sudden pipe bursts. Two cases, pipeline and pipe network, are analysed in parallel throughout the thesis. In the first part of this chapter, the summary of the obtained results is given. Guidelines for future research are discussed in the second part of the chapter.

7.1 Summary of results

The results of the presented work can be divided into three parts. First part is the technique for burst detection and location in pipelines. Second part is the technique for burst detection and location in pipe networks. The third part is the implementation of the transient solver.

Burst detection and location in pipelines

A novel approach for detecting and locating sudden pipeline bursts was presented. The technique is based on analysis of the continuous pressure measurement at one point along the pipeline. In case of a burst event, the burst-induced wave and its reflections from the pipeline boundaries are analysed and the location of the burst determined. The method shows promise for efficient detection and location of bursts in pipelines. Both laboratory and field validation confirms the

approach taken for fast bursts. Due to the fact that only a single point pressure measurement is required, the cost of installation of such a monitoring system is quite low. Although the technique was derived considering an application in water mains, it can also be used for burst detection and location in other fluid-carrying pipelines.

Burst detection and location in pipe networks

A fluid transient-based continuous monitoring technique for detecting and locating bursts in pipe networks was presented. Two or more pressure measurements are used to detect burst and derive its location. Sub-algorithms for measurement location selection and change detection in pressure data were presented. Verified using simulated data, the algorithm provides promising results for a small-scale network. The algorithm can successfully detect, locate and size the bursts that occur at the nodes in the network or along the pipes in the network. Based only on pressure measurements, it does not require complex equipment or large investments. Also, since simple wave transmission theory is used, it is not necessary to simulate the whole network, which leads to greater efficiency. Such a tool will potentially provide early warning for system failures, which would help to avoid losses of water and interruptions of service.

Transient simulation

A code was implemented for solving governing unsteady flow equations. The explicit Method of Characteristics (MOC) scheme is used. The boundary equations are included for leak and burst as well as the basic boundaries. The unsteady friction model is implemented to represent the effect of frequency dependent friction. The code is integrated with the interface of EPANET steady state hydraulic solver, which provides a convenient way for building the network models and allows quick changes of parameters as well as provides initial head and flow values for transient simulation.

7.2 Future work

There are still a number of problems that are subjects for future work. In this section, the main directions for continuation of the work presented in this thesis are given.

Detection and location of slower bursts

The presented approaches are valid for sudden pipe bursts. Although, it is likely that most bursts will occur rapidly, slower events have to be considered. An additional pressure monitoring point might be necessary to detect and locate slower bursts in pipelines. As an alternative, ancillary techniques, such as inverse transient analysis (Liggett and Chen; 1994) and transient damping methods (Wang et al.; 2002), which use more information from the transient signal, could be employed to determine the location and size of the burst.

Including operational transients

At the present state, transients induced by operations of pumps and valves are not included in the analysis. The burst monitoring is disabled during "normal" transients. In certain situations, "normal" transients can be the reason of the burst. Thus, it would be beneficial to extend the approach so that transients caused by normal operation are accounted for. This could be done by modelling "normal" transients and observing the discrepancy between the simulated and measured pressure traces.

Experimental verification

So far, the burst detection and location algorithm for pipe networks has been verified using the simulated data. The next step is to carry out experimental tests. The field validation is an important part of the future work.

Extension for large networks

The technique has proven to be effective for small-scale networks. In real applications, the network can be significantly more complex, which implies that more pressure monitoring points will be necessary. The optimal placing of pressure monitoring sites is an important point that must be addressed in a separate analysis. Having more measurement points throughout the network, burst-induced transient waves might be detected at more than two of them. The precision of burst location might be increased by analysing wave arrival times at all the nodes where wave is detected.

Bibliography

Andersen, J. and Powell, R. (2000). Implicit state-estimation technique for water network monitoring, *Urban Water* **2**: 123–130.

Arfaie, M., Suwan, K. and Anderson, A. (1993). Stability and accuracy of pipe friction approximations in method of characteristics solutions for waterhammer, *Mathematical Engineering in Industry* **1**(4): 265–281.

Åström, K. and Wittenmark, B. (1997). *Computer-Controlled Systems: theory and design*, 3rd edn, Prentice-Hall, Inc., Engelwood Cliffs, New Jersey, USA.

AWWA (1999). Water meters-selection, installation, testing and maintenance, *Document M6 1-58321-017-02*, American Water Works Association, Denver, Colorado, USA.

Basseville, M. and Nikiforov, I. (1993). *Detection of Abrupt Changes: Theory and Applications*, Prentice-Hall, Inc., Englewood Cliffs, New Jersey, USA.

Benkherouf, A. and Allidina, A. (1988). Leak detection and location in gas pipelines, *IEE Proceedings* **135**(2): 142–148.

Bergant, A. and Simpson, A. (1995). Water hammer and column separation measurements in an experimental apparatus, *Research Report R128*, School of Civil and Environmental Engineering, University of Adelaide, Adelaide, Australia.

Brunone, B. (1999). Transient test-based technique for leak detection in outfall pipes, *Journal of Water Resources Planning and Management, ASCE* **125**(5): 302–306.

Brunone, B. and Ferrante, M. (2001). Detecting leaks in pressurised pipes by means of transients, *Journal of Hydraulic Research, IAHR* **39**(5): 539–547.

Cowan, G. (1975). Digital processing adds accuracy to TDR, *Microwaves* pp. 47– 51.

Emara-Shabaik, H., Khulief, Y. and Hussaini, I. (2002). A non-linear multiple-model state estimation scheme for pipeline leak detection and isolation, *Proc. Inst. Mech. Eng. Part I: Journal of Systems and Control Engineering* **216**(6): 497–512.

EUREAU (2001). Losses from water distribution networks, *EUREAU Position Paper EU1-01-A66(5)*, EUREAU.

Ferrante, M. and Brunone, B. (2003a). Pipe system diagnosis and leak detection by unsteady-state tests. 1. Harmonic analysis, *Advances in Water Resources* **26**: 95–105.

Ferrante, M. and Brunone, B. (2003b). Pipe system diagnosis and leak detection by unsteady-state tests. 2. Wavelet analysis, *Advances in Water Resources* **26**: 107–116.

Ghidaoui, M., Karney, B. and McInnis, D. (1998). Energy estimates for discretization errors in water hammer problems, *Journal of Hydraulic Engineering, ASCE* **124**(4): 384–393.

Golby, J. and Woodward, T. (1999). Find that leak, *IEE Review* **45**(5): 219–221.

Greco, M. and Carravetta, A. (1999). Water hammer in branched networks, 28^{th} *IAHR congress*, Graz, Austria.

Harding, R. (1976). Use pulse instead of CW signals, *Electrical Design* **11**: 60–67.

Isermann, R. (1984). Process fault detection based on modeling and estimation methods - a survey, *Automatica* **20**(4): 387–404.

Jönsson, L. (1995). Hydraulic transients as a monitoring device, *Technical report*, Dept. of Water Resources Engineering, University of Lund, Lund, Sweden.

Jönsson, L. (2001). Interaction of a hydraulic transient with a leak in a pipe flow, 14^{th} *Australasian Fluid Mechanics Conference*, Adelaide University, Adelaide, Australia.

Jönsson, L. and Larson, M. (1992). *Pipeline Systems*, Kluwer Academic Publishers, chapter Leak detection through hydraulic transient analysis, pp. 273–286.

Karney, B. and Ghidaoui, M. (1997). Flexible discretization algorithm for fixed-grid moc in pipelines, *Journal of Hydraulic Engineering, ASCE* **123**(11): 1004–1011.

Khan, A., Widdop, P., Day, A., Wood, A., Mounce, S. and Machell, J. (2002). Low-cost failure sensor design and development for water pipeline distribution systems, *Water Science and Technology* **45**(4-5): 207–216.

Khomsi, D., Walters, G., Thorley, A. and Ouazar, D. (1996). Reliability tester for water-distribution networks, *Journal of Computing in Civil Engineering* **10**(1): 10–19.

Kiuchi, T. (1993). A leak localization method of pipeline by means of fluid transient model, *Journal of Energy Resources Technology, ASME* **115**: 162–167.

Kiuchi, T., Izumi, H. and Huke, T. (1995). An operation support system of large city gas networks based on fluid transient model, *Journal of Energy Resources Technology, ASME* **117**: 324–328.

Kleiner, Y. and Rajani, B. (2001). Comprehensive review of strucural deterioration of water mains: statistical models, *Urban Water* **3**: 131–150.

Lambert, A. and Hirner, W. (2000). Losses from water supply systems: standard terminology and recommended performance measures, *The blue pages*, IWA, London, UK.

Lee, P., Simpson, A., Lambert, M., Vítkovský, J. and Misiunas, D. (2003a). Leak location in pipelines using transient reflection, *Submitted to ASCE*.

Lee, P., Vítkovský, J., Lambert, M., Simpson, A. and Liggett, J. (2003b). Frequency response coding for the location of leaks in single pipeline systems, *in*

E. Cabrera and E. C. Jr. (eds), *Pumps, Electromechanical Devices and Systems Applied to Urban Water Management*, Valencia, Spain.

Liggett, J. and Chen, L. (1994). Inverse transient analysis in pipe networks, *Journal of Hydraulic Engineering, ASCE* **120**(8): 934–955.

Liou, J. and Tian, J. (1995). Leak detection - transient flow simulation approaches, *Journal of Energy Resources Technology, Trans. ASME* **117**(3): 243–248.

Loganathan, G., Park, S. and Sherali, H. (2002). Threshold break rate for pipeline replacement in water distribution systems, *Journal of Water Resources Planning and Management* **128**(4): 271–279.

Misiunas, D. (2001a). Drinking water quality. Literature study on water distribution systems, *Technical report TEIE-7169*, Dept. of Industrial Electrical Engineering and Automation, Lund University, Lund, Sweden.

Misiunas, D. (2001b). Dynamic behaviour of a pump/pipeline system. Literature study on water distribution systems, *Technical report TEIE-7166*, Dept. of Industrial Electrical Engineering and Automation, Lund University, Lund, Sweden.

Misiunas, D. (2001c). Leakage control. Literature study on water distribution systems, *Technical report TEIE-7167*, Dept. of Industrial Electrical Engineering and Automation, Lund University, Lund, Sweden.

Misiunas, D. (2001d). Water storage. Literature study on water distribution systems, *Technical report TEIE-7168*, Dept. of Industrial Electrical Engineering and Automation, Lund University, Lund, Sweden.

Misiunas, D. (2002). Integrated information and operation systems in urban water infrastructure - leakage control, *Technical report TEIE-7172*, Dept. of Industrial Electrical Engineering and Automation, Lund University, Lund, Sweden.

Misiunas, D., Vítkovský, J., Olsson, G., Simpson, A. and Lambert, M. (2003). Pipeline burst detection and location using a continuous monitoring technique, *International Conference on Advances in Water Supply Management, CCWI*, Imperial College London, UK, pp. 89–96.

Misiunas, D., Vítkovský, J., Olsson, G., Simpson, A. and Lambert, M. (2004). Burst detection and location in pipe networks using a continuous monitoring technique, 9^{th} *International Conference on Pressure Surges*, Chester, UK. accepted for publication.

Mounce, S., Day, A., Wood, A., Khan, A., Widdop, P. and Machell, J. (2001). A neural network approach to burst detection, *1-st IWA Conference on Instrumentation, Control and Automation (ICA2001)*, Vol. 1, Malmö, Sweden, pp. 349–356.

Mounce, S., Khan, A., Wood, A., Day, A., Widdop, P. and Machell, J. (2003). Sensor-fusion of hydraulic data for burst detection and location in a treated water distribution systems, *Information Fusion* (4): 217–119.

Mukherjee, J. and Narasimhan, S. (1996). Leak detection in networks of pipelines by generalized likelihood ratio method, *Industrial & Engineering Chemistry Research* **35**(6): 1886–1893.

Nash, G. and Karney, B. (1999). Efficient inverse transient analysis in series pipe systems, *Journal of Hydraulic Engineering, ASCE* **125**(7): 761–764.

OFWAT (2001). Leakage figures, *Technical report*, Birmingham, UK.

Page, E. (1954). Continuous inspection schemes, *Biometrika* **41**: 100–115.

Pelletier, G., Mailhot, A. and Villeneuve, J.-P. (2003). Modelling water pipe breaks - three case studies, *Journal of Water Resources Planning and Management, ASCE* **129**(2): 115–123.

Poulakis, Z., Valougeorgis, D. and Papadimitriou, C. (2003). Leakage detection in water pipe networks using a bayesian probabilistic framework, *Probabilistic Engineering Mechanics* **18**: 315–327.

Rajani, B. and McDonald, S. (1995). Water mains break data for different pipe materials for 1992 and 1993, *Technical report*, National Research Council of Canada.

Rajtar, J. and Muthiah, R. (1997). Pipeline leak detection system for oil and gas flowlines, *Journal of Manufacturing Science and Engineering, Trans. ASME* **119**(1): 105–109.

Rossman, L. (2000). EPANET users manual, *Technical report*, Risk Reduction Engineering Laboratory, Cincinnati: EPA, USA.

Schlattman, D. (1991). Pressure analysis improves lines' leak-detection capabilities, *Oil & Gas Journal* **89**(52): 98–101.

Silva, R., Buiatta, C., Cruz, S. and Pereira, J. (1996). Pressure wave behaviour and leak detection in pipe-lines, *Computers in Chemical Engineering* **20**: 491–496.

Stapers, R. J. J. (2002). Urban water distribution. leak detection and model calibration in complex pipe networks, *Technical report TEIE-7170*, Dept. of Industrial Electrical Engineering and Automation, Lund University, Lund, Sweden.

Tao, L. and Wang, C. (1988). State estimation of output-decoupled complex system with application to fluid pipeline, *IEEE Transactions on Industrial Electronics* **35**(3): 469–475.

Vardy, A. and Brown, J. (1996). On turbulent, unsteady, smooth-pipe friction, 7^{th} *International Conference on Pressure Surges and Transients in Pipelines and Open Channels*, BHR Group, Harrogate, UK, pp. 289–311.

Vardy, A. and Brown, J. (2003). Transient turbulent friction in fully-rough pipe flows, *Journal of Sound and Vibration*. In press.

Vítkovský, J., Simpson, A. and Lambert, M. (1999). Leak detection and calibration of water distribution system using transient and genetic algorithms, *Water Distribution System Conference*, Division of Water Resource Planning and Management, ASCE, Tempe, Arizona, USA.

Vítkovský, J., Simpson, A., Lambert, M. and Wang, X. (2001). An experimental verification of the inverse transient technique, *6th Conference on Hydraulics in Civil Engineering*, I.E.Aust., Hobart, Australia, pp. 373–380.

Vugdelija, M., Stojanovic, Z. and Stojanovic, Z. (2000). Determination of a time step interval in hydraulic systems transients simulation, *Advances in Engineering Software* **31**(2): 143–148.

Wang, G., Dong, D. and Fang, C. (1993). Leak detection for transport pipelines based on autoregressive modeling, *IEEE Transactions on Instrumentation and Measurement* **42**(1): 68–71.

Wang, X., Lambert, M., Simpson, A. and Vítkovský, J. (2001). Leak detection in pipelines and pipe networks: a review, 6^{th} *Conference on Hydraulics in Civil Engineering*, I.E. Aust., Hobart, Australia, pp. 391–400.

Wang, X., Lambert, M., Simpson, A., Liggett, J. and Vítkovský, J. (2002). Leak detection in pipeline systems using the damping of fluid transients, *Journal of Hydraulic Engineering, ASCE* **128**(7): 697–711.

Whaley, R. S., Nicholas, R. E. and Reet, J. V. (1992). A tutorial on software based leak detection methods, *Technical report*, Pipeline Simulation Interest Group, Houston, USA.

Wylie, E. (1983). The microcomputer and pipeline transients, *Journal of Hydraulic Engineering, ASCE* **109**(12): 1723–1739.

Wylie, E. and Streeter, V. (1993). *Fluid Transients in Systems*, Prentice-Hall, Inc., Engelwood Cliffs, New Jersey, USA.

Zhang, J. (2001). Statistical pipeline leak detection for all operating conditions, *Pipeline and Gas Journal* **229**(2): 42–45.

Zielke, W. (1968). Frequency-dependent friction in transient pipe flow, *Journal of Basic Engineering, Trans. ASME Series D* **90**: 109–115.

Nomenclature

A	Cross-sectional pipe area
a	Wave speed
B	Pipe characteristic impedance
$C_d A_0$	Lumped burst orifice coefficient
D	Pipe diameter
E	Young's modulus of elasticity of conduit walls
e	Pipe wall thickness
f	Friction factor
g	Gravitational acceleration
g_t	CUSUM variable
H	Hydraulic head
h	CUSUM threshold parameter
H_0	Initial head in pipeline
K	Bulk modulus of elasticity of fluid
L	Pipeline length
N	Number of nodes in network

n	CUSUM drift parameter
P	Reflection coefficient
Q	Volumetric flow rate
R	Pipe resistance coefficient
Re	Reynolds number
S	Objective function for burst location
s	Score variable for burst location
T	Transmission coefficient
t	Time
t_a	Time of CUSUM alarm
t_B	Time of burst event
t_M	Time for wave to travel from measurement point to boundary and return
T_W	Post-alarm analysis window length
T_ϵ	Pre-alarm analysis window length
T_{sum}	Optimal measurement location variable
V	Mean velocity of the flow
w	Weighting factor
x_B	Burst location (as a fraction of pipeline length)
x_M	Measurement location (as a fraction of pipeline length)
y	Raw signal
y_t	RLS filter measured input signal
ΔH	Head change due to burst

Δt	Time difference
Δx	Length of computational unit
λ	RLS filter forgetting factor
∂	Partial derivative
ϕ	Parameter in wave speed equation depending on the pipe anchoring
ρ	Fluid density
τ	Wave travel time
θt	RLS filter output signal
ε_t	RLS filter prediction error

CUSUM	Cumulative sum
DMA	District metering area
ITM	Inverse transient method
MOC	Method of characteristics
RLS	Recursive least squares
SCADA	Supervisory control and data acquisition
TDR	Time domain reflectometry
UFW	Unaccounted for water

Appendix A

Experimental work

In this appendix, the experimental work of this thesis is described. Two sets of experiments were performed. The first set of tests was carried out using a laboratory pipeline. The second set was conducted in field conditions. The results of these experiments are analysed in Chapter 5. In the following two sections descriptions of the experimental sites, equipment used and tests undertaken are given.

A.1 Laboratory experiments

Apparatus

The experimental single pipeline in the Robin Hydraulics Laboratory in the School of Civil and Environmental Engineering at The University of Adelaide, Australia was used for laboratory verification of the pipeline burst detection and location technique. Figure A.1 shows the principal scheme of the pipeline. It is composed of a 37.527 m long copper pipe with an inside diameter of 22.1 mm and a wall thickness of 1.6 mm. A photograph of the pipeline is shown in Figure A.2. There are 5 brass blocks along the pipeline (points A, B, C, D and E in Figure A.1). These blocks are used as connection points for pressure transducers and side-discharge valves. There is a ball valve at each end of the pipeline.

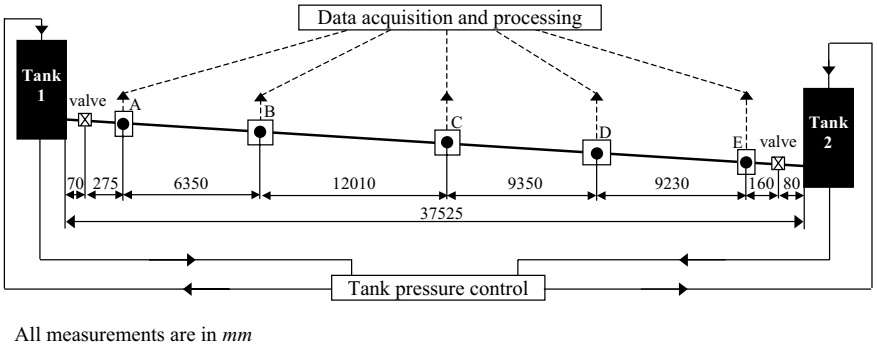

Figure A.1: Experimental pipeline.

Figure A.2: Overall layout of the pipeline.

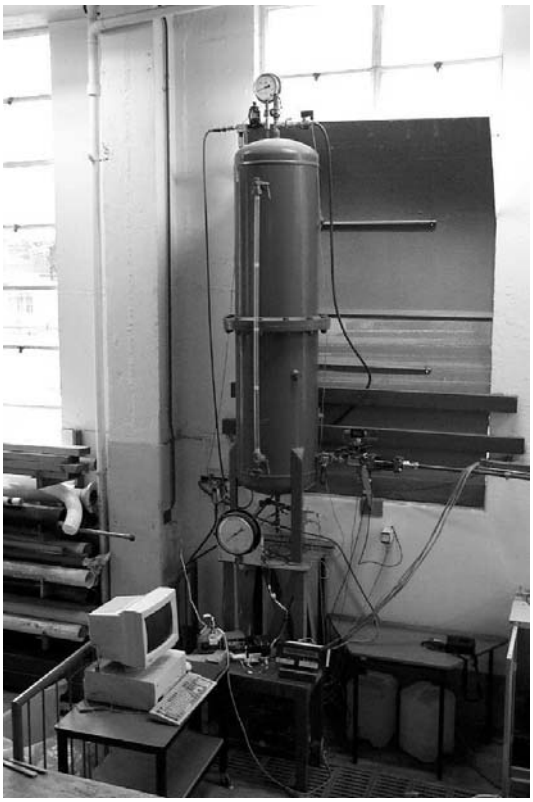

Figure A.3: Boundary tank and data acquisition system.

Two pressurised tanks at each end of the pipeline control the steady state pressure and flow. The difference in tank elevation is 2 m. The pressure is regulated by a computer control system. The maximum pressure of each tank is 70 m of head. A photograph of one tank is shown in Figure A.3.

The pressure is measured using Druck flush fit pressure transducers. The flush fit prevents undesirable effects of the transducers interference with the fluid flow. The rise time of the transducers is 5×10^{-6} s. The absolute pressure range is 0 to 600 kPa and the uncertainty is $\pm 0.1\%$ of full span. The transducers are mounted in brass blocks. Figure A.4 shows a photograph of the transducer and the brass block. An amplifier is needed to amplify the measured pressure signal.

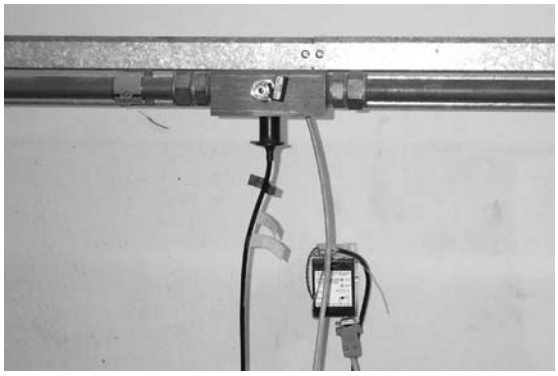

Figure A.4: Pressure transducer with brass block.

The data acquisition is performed on a 150 MHz Pentium computer using an Intelligent Instrumentation data acquisition card and visual designer software (see Figure A.3).

The burst is simulated by opening a solenoid side-discharge valve (see Figure A.5). The calibrated lumped discharge parameter of the solenoid is $C_d A_0 = 1.7665 \times 10^{-6}$ m^2 and the opening time is 4 ms. The manual opening of a side discharge valve can also be used to simulate a burst. In that case, $C_d A_0 = 6.0192 \times 10^{-7}$ m^2 and the estimated opening time is 30 ms.

Experiments

The burst was simulated by triggering the solenoid valve a short time after the pressure measurement was started. Four different burst locations were tested – points B (test 1), C (test 2), D (test 3), and E (test 4) according to Figure A.1. The pressure transducer was placed at point B for all the tests. The measurements were sampled with a sampling frequency of 2 kHz. The calibrated wave speed of the pipeline was 1327 m/s. In Figure A.6, the collected pressure traces are shown. An additional test was performed using a manual side discharge valve (1 mm) opening for slow burst simulation. The burst was located at point B and the pressure transducer was placed at point D (refer to Figure A.1). The measured trace is shown in Figure A.7.

Figure A.5: The solenoid valve.

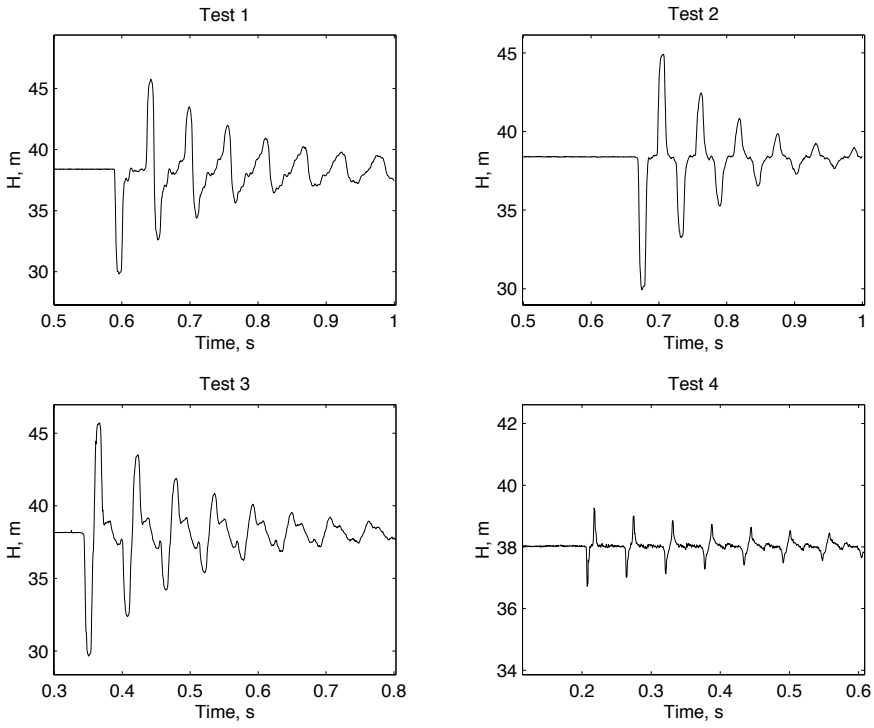

Figure A.6: The pressure traces from tests 1 to 4.

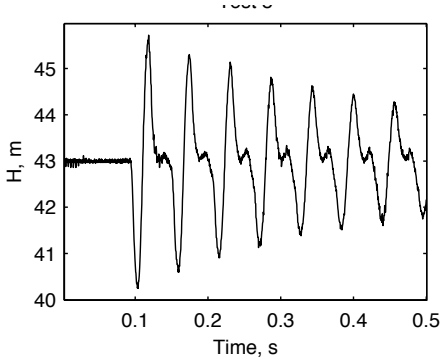

Figure A.7: Pressure trace from test 5.

A.2 Field experiments

The site

The field experiments were performed on a single pipe branch of the Willunga network. Willunga is a township located on the southern edge of metropolitan Adelaide, South Australia. The selected pipe is 356.53 m long and has a diameter of 100 mm. It has a dead-end as one boundary and is connected to the rest of the network by a tee-junction at the other side. The layout of the pipe, together with the elevation distribution, are shown in Figure A.8. The fire hydrant connections correspond to the points A, B, C, E and F in the figure.

The pressure sensor plugs

Connection to the pipe was made through the fire hydrant plugs. The usual distance between two fire plugs in water distribution network is less than 100 meters. A fire hydrant plug comprises a valve chamber, which allows a standpipe or hose connection to be made. Special fire hydrant caps incorporating 60 bar (6000 kPa) Druck pressure transducers were produced for experiments. The transducers are placed in such way that the transducer face is exposed to the flow stream in the pipe beneath the fire hydrant plug. This setup allowed measuring the pressure within the pipe. Figure A.9 shows a connected pressure sensor plug.

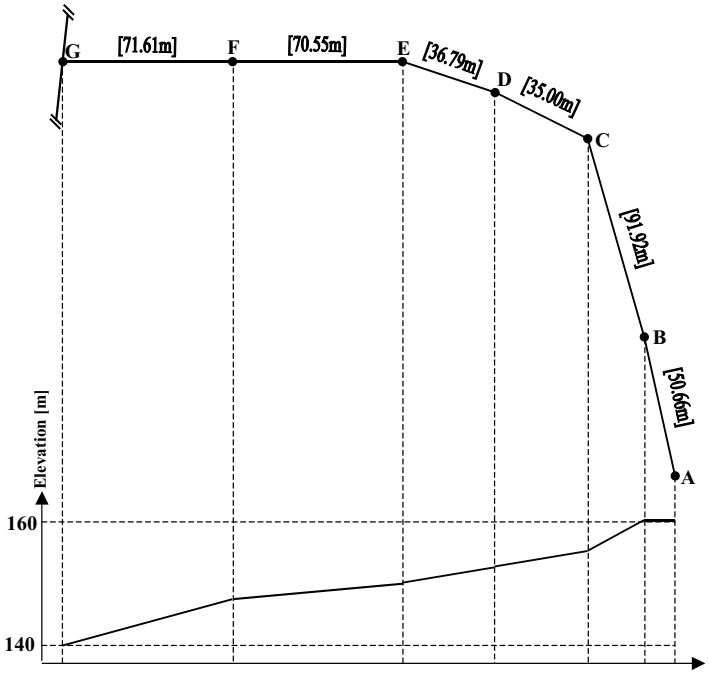

Figure A.8: The layout and elevation of the field pipe.

Figure A.9: The connected fire hydrant cap with incorporated transducer.

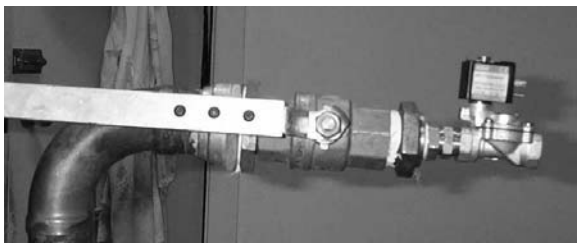

Figure A.10: The solenoid valve connected to the standpipe.

Figure A.11: Experimental burst.

The burst generator

To simulate a pipe burst the sudden opening of the discharge through the fire plug was used. A solenoid valve was used as a burst generator (see Figure A.10). The valve was attached to the end of a standpipe connected to a fire hydrant plug. The burst generation can be observed in Figure A.11. The internal diameter of the solenoid valve is 10 mm, which results in the lumped discharge parameter $C_d A_0 = 5.4978 \times 10^{-5}$ m^2.

Figure A.12: The data acquisition system.

Data acquisition system

The DASPort high speed data acquisition unit (Intelligent Instruments) was used for collecting pressure measurement data. The unit is compatible with Visual Designer software. Measured data is stored in the disc drive of the computer. Batteries are used as a power supply. The connected data acquisition system is shown in Figure A.12.

Synchronization of measurements

The wave speed value for the pipe was obtained from the measurement of wave travel times between two measurement points. Such experiment requires synchronization of two pressure measurements. Each measurement station comprises a pressure transducer, DASPort unit and portable computer, which means that the measurements could only be synchronised to the resolution of the internal clock in each computer. The resolution of the computers used is in the range of 50 ms to 0.5 s. This is not adequate, considering that the wave speed usually is more than 1000 m/s. Using the internal computer clock could result into $5 - 50\%$ error of estimated wave speed value. This problem was solved by connecting both measurement stations to a common cable and sending a voltage trigger before starting a test. The voltage change reaches both stations

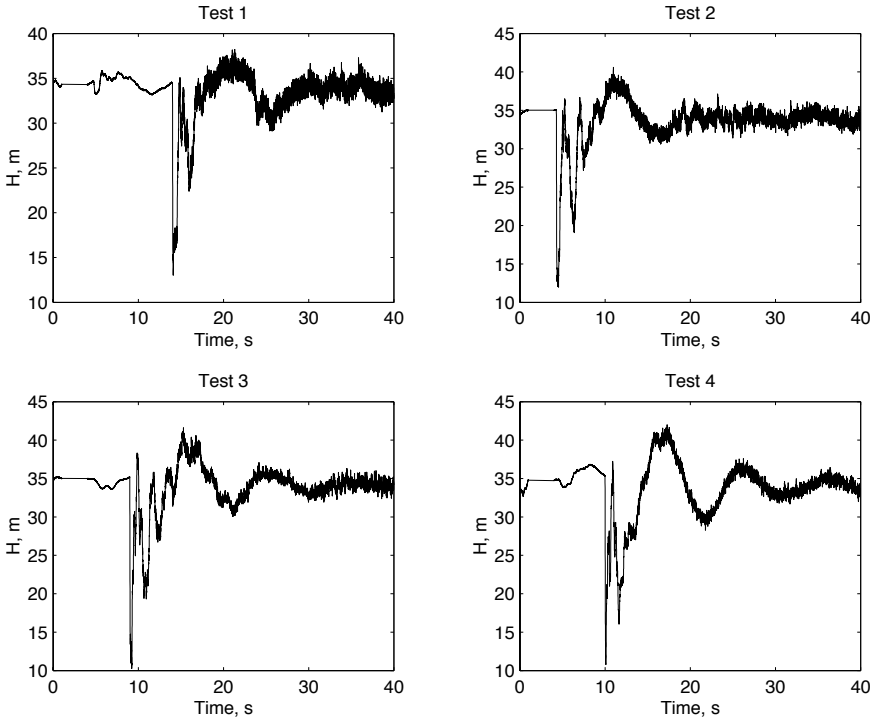

Figure A.13: Pressure recorded at point A (dead-end) for tests 1 to 4

simultaneously in less than one millisecond. The Visual Designer program has been modified to record the voltage signal. In this way, the error in synchronisation is limited to one sampling period.

Experiments

The fire hydrant plugs were flushed prior to testing. This is done in order to release the accumulated air and sediment. Four tests were conducted. A standpipe with a solenoid was placed at different positions along the pipeline to simulate different locations of the burst. The tests were performed in the same manner as the laboratory experiments. The solenoid valve was actuated shortly time after the measuring was started. In this case, the pressure was

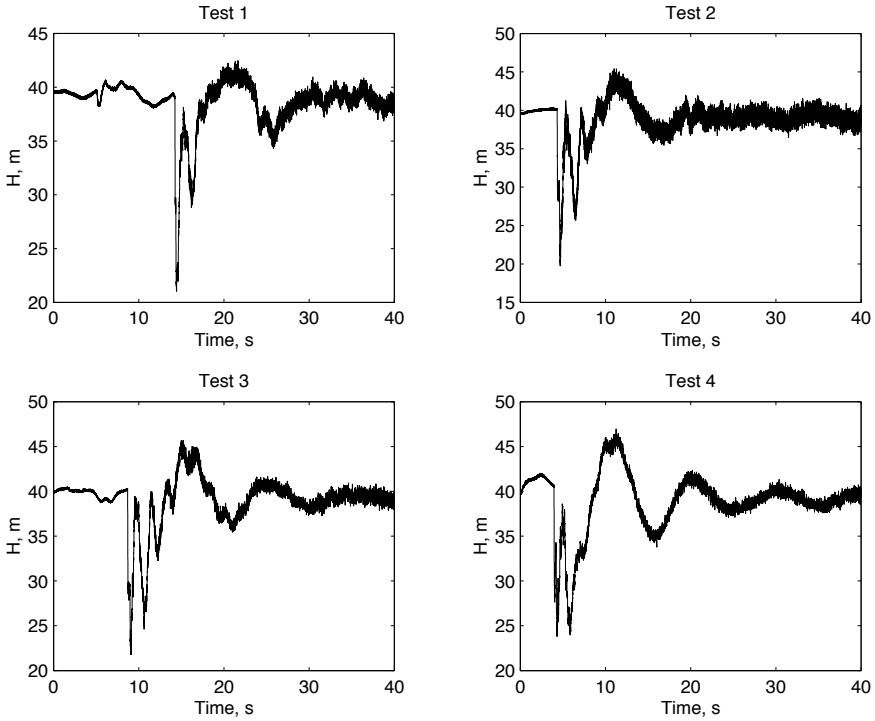

Figure A.14: Pressure recorded at point C (142.58m away from the dead-end) for tests 1 to 4

measured at two positions (points A and C in Figure A.8) simultaneously. The wave speed value was calculated from the transient wave travel time between two measurement points and was equal to 1150 m/s. The burst was located at points B (test 1), C (test 2), E (test 3), and F (test 4). Figures A.13 and A.14 show pressure traces measured at points A and C respectively. The measurements were sampled with a 500 Hz sampling frequency.

Appendix B

Pressure wave transmission and reflection coefficients

When a transient pressure wave interacts with a junction of two or more pipes, a certain part of the wave is transmitted through the junction and the rest of the wave is reflected. The wave transmission and reflection coefficients can be derived using the compatibility equations from the Method of Characteristics. An example of a three pipe junction is used (Figure B.1). The continuity equation for the junction before the wave reaches it (time $t - \Delta t$) is:

$$Q_{01} = Q_{02} + Q_{03} \tag{B.1}$$

The continuity equation for the junction after the wave has reached it (time $t + \Delta t$) is:

$$Q_{J1} = Q_{J2} + Q_{J3} \tag{B.2}$$

The head at junction H_0 is common for all the pipes. Assuming that the pressure wave enters the junction from pipe 1, the head in pipe 1 is increased from H_0 to H_W. The corresponding flow Q_W can be calculated using the C^-compatibility equation:

$$H_w = H_0 + B_1(Q_w - Q_{01}) \tag{B.3}$$

and is equal to:

$$Q_w = Q_{01} + \frac{1}{B_2}(H_w - H_0) \tag{B.4}$$

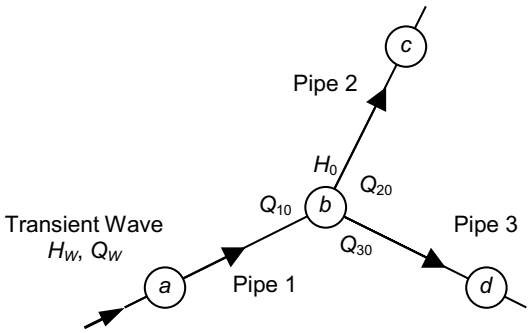

(a) Layout of three-pipe junction example

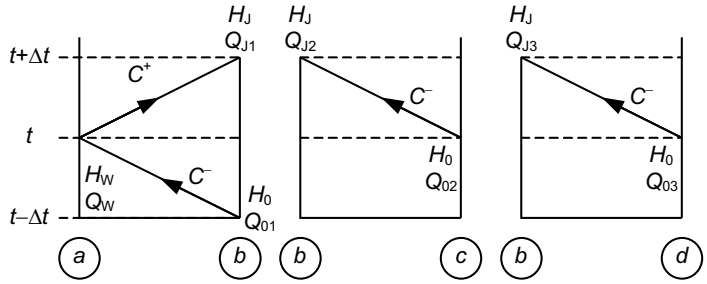

(b) Characteristic Grids for three-pipe junction example

Figure B.1: The layout and characteristic grid for the three-pipe junction example.

where B_1 is the characteristic impedance of pipe 1:

$$B = \frac{a}{gA} \tag{B.5}$$

When the pressure wave reaches a junction, the conditions at that junction are described by the following compatibility equations:

$$H_j = H_W - B_1(Q_{J1} - Q_W) \tag{B.6}$$
$$H_j = H_0 + B_2(Q_{J2} - Q_{02}) \tag{B.7}$$
$$H_j = H_0 + B_3(Q_{J3} - Q_{03}) \tag{B.8}$$

Substituting B.4 into B.6 and rearranging B.7 and B.8 results in:

$$Q_{J1} - Q_{01} = \frac{1}{B_1}(2H_w - H_0 - H_J) \tag{B.9}$$
$$Q_{J2} - Q_{02} = \frac{1}{B_2}(H_J - H_0) \tag{B.10}$$
$$Q_{J3} - Q_{03} = \frac{1}{B_3}(H_J - H_0) \tag{B.11}$$

Subtraction of B.1 from B.2 gives:

$$(Q_{J1} - Q_{01}) = (Q_{J2} - Q_{02}) + (Q_{J3} - Q_{03}) \tag{B.12}$$

Finally, substituting B.9, B.10 and B.11 into B.12 and rearranging the equation gives:

$$\frac{H_w - H_0}{H_J - H_0} = \frac{\dfrac{2}{B_1}}{\dfrac{1}{B_1} + \dfrac{1}{B_2} + \dfrac{1}{B_3}} \tag{B.13}$$

Figure B.2 illustrates the pressures in all three pipes connected to the junction after the wave has passed the junction.

If a general junction n of P pipes is considered, the wave transmission coefficient T_n, in the case when the wave is approaching from pipe 1, is equal to:

$$T_n = \frac{(H_J - H_0)}{(H_W - H_0)} = \frac{\dfrac{2}{B_1}}{\displaystyle\sum_{k=1}^{P} \frac{1}{B_k}} \tag{B.14}$$

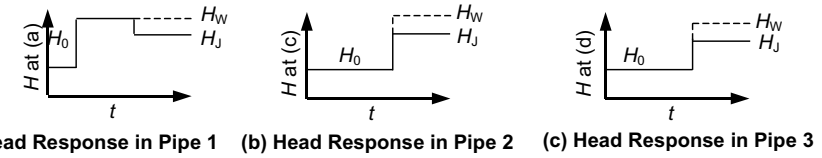

Figure B.2: Head responses of the three pipes.

By substituting B.5 into B.14, the following expression is obtained:

$$T_n = \frac{\frac{2A_1}{a_1}}{\sum_{k=1}^{P} \frac{A_k}{a_k}} \tag{B.15}$$

Thus, the transmission coefficient for a junction depends on the properties of the pipes connected to it. The part of the transient wave that is not transmitted is reflected. The reflection coefficient is defined as:

$$P_n = \frac{(H_J - H_W)}{(H_W - H_0)} = T_n - 1 \tag{B.16}$$

Equation B.15 is valid for any junction connecting two or more pipes. It can also be applied to situations when pipes with different diameters or wave speeds are connected in series. In the same manner, the transmission and reflection coefficients for the most common boundaries can be derived.

Reservoir The reservoir can be treated as a pipe with $A \rightarrow \infty$. This results in $T = 0$ and $P = -1$. In other words, the wave is reflected with the same magnitude and opposite sign, which means that the initial pressure is restored after reflection.

Dead-end Flow is equal to zero at the dead-end of the pipe. Thus, $T = 0$ and by solving the characteristic equations the reflection coefficient $P = 1$ is derived. The reflected wave has the same magnitude and same sign, which means that head is amplified at the dead-end. The same reasoning is valid for the negative transient wave – it is further reduced at the boundary.

Appendix C

Calculation of burst size

In 1897, Joukowsky found a special solution of the governing unsteady pipe flow equations for the case of instantaneous valve closure. He formulated the expression, named the Joukowsky pressure rise formula, which related the change in velocity to the resulting change in pressure. The convective terms and frictional resistance are neglected and the pipe is assumed to be horizontal. The pressure rise formula can be applied only when the change in velocity is faster than the time it takes for the burst-induced wave to reach the induction point after reflection from the boundary. For closure of a valve at the downstream end of a pipeline, a change in velocity ΔV must occur in less that $2L/a$ seconds, where L is the length of the pipeline. The Joukowsky rise in head is calculated from the following formula:

$$\Delta H = -\frac{a}{g}\Delta V \tag{C.1}$$

By substituting velocity with flow ($V = QA$) Equation C.1 becomes

$$\Delta H = -\frac{a}{gA}\Delta Q \tag{C.2}$$

As already noted, this relation is valid for the instantaneous downstream valve closure. This means that the transient wave initiated by a sudden pressure rise will be travelling in one direction (upstream from the valve). In the case of a burst event somewhere along the pipe, the sudden change in flow (velocity) is

caused by a side discharge through the burst orifice and is equal to the burst flow Q_B. The impedance of pipe sections immediately upstream and downstream of the burst is equal. Therefore, the upstream and downstream flows after the burst occurs are:

$$Q_u = Q_0 + \frac{1}{2}Q_B \tag{C.3}$$

$$Q_u = Q_0 - \frac{1}{2}Q_B \tag{C.4}$$

respectively. It is important to realise that the Joukowsky formula was derived for a pressure wave propagating upstream. Applying Equation C.2 at any point upstream from the burst gives:

$$\Delta H_{Bu} = -\frac{a}{gA}\left[Q_0 - (Q_0 + \frac{1}{2}Q_B)\right] \tag{C.5}$$

and, after rearranging:

$$\Delta H_B u = -\frac{aQ_B}{2gA} \tag{C.6}$$

The same analysis can be applied for the wave propagating downstream. In this case, the Joukowsky formula has the following form:

$$\Delta H = \frac{a}{gA}\Delta Q \tag{C.7}$$

Applying the above equation at any point downstream from the burst gives:

$$\Delta H_{Bd} = \frac{a}{gA}\left[Q_0 - (Q_0 - \frac{1}{2}Q_B)\right] \tag{C.8}$$

and, after rearrangement:

$$\Delta H_{Bd} = -\frac{aQ_B}{2gA} \tag{C.9}$$

From Equations C.6 and C.9 it appears that $\Delta H_{Bu} = \Delta H_{Bd}$. This means that negative pressure waves of equal magnitude ΔH_B travel in opposite directions away from the burst point:

$$\Delta H_B = -\frac{aQ_B}{2gA} \tag{C.10}$$

The burst flow can be calculated using the orifice equation:

$$Q_B = C_d A_0 \sqrt{2gH_B} \tag{C.11}$$

where $C_d A_0$ is a lumped discharge parameter describing the size of the burst and H_B is the head at the burst point. Solving Equation C.10 for burst flow Q_B gives:

$$Q_B = -\frac{2gA}{a}\Delta H_B \tag{C.12}$$

After substituting Equation C.12 into Equation C.11 the expression for the burst size calculation is derived:

$$C_d A_0 = -\frac{A\Delta H_B \sqrt{2g}}{a\sqrt{H_B}} \tag{C.13}$$

Considering that a burst orifice discharge Q_B will always be positive and pressure change ΔH_B will always be negative (from Equation C.10) Equation C.13 can be rewritten as:

$$C_d A_0 = \frac{A|\Delta H_B|\sqrt{2g}}{a\sqrt{H_B}} \tag{C.14}$$

ΔH_B is the magnitude of the burst-induced pressure wave (from the pressure measurement). The head at the burst point H_B can be found by subtracting ΔH_B from the initial head value H_0:

$$H_B = H_0 - \Delta H_B \tag{C.15}$$

Equation C.13 does not provide the exact size of the burst due to the neglection of frictional effects. However, it still provides a reasonable estimate, which can be used to evaluate the severity of the burst.